Automated Operational Modal Analysis of a Cable-Stayed Bridge

Miao Sun [1], Mehrisadat Makki Alamdari [2], Hamed Kalhori [3]

[1] Research Assistant, CSIRO, Data61, 13 Garden Street, Eveleigh NSW 2015, Australia, smiaos@hotmail.com

[2] Post-doctoral Researcher, CSIRO, Data61, 13 Garden Street, Eveleigh NSW 2015, Australia (Corresponding author), Mehri.Makkialamdari@data61.csiro.au

[3] Research Assistant, CSIRO, Data61, 13 Garden Street, Eveleigh NSW 2015, Australia Hamed.kalhori@data61.csiro.au

Abstract

Automated techniques for analyzing the dynamic behavior of full-scale civil structures are becoming increasingly important for continuous structural health monitoring applications. This paper aims to extract the structural modal parameters of a full-scale cable-stayed bridge from the collected 'output-only' vibration data without the need of any user interactions. The work focuses on the development of an automated and robust operational modal analysis (OMA) algorithm, utilizing a multi-stage clustering approach. The main contribution of the work is to define a novel way of automatically defining the hierarchical clustering threshold to enable the accurate identification of a complete set of modal parameters. The proposed algorithm is demonstrated to work with any parametric system identification algorithm that uses the system order '*n*' as the sole parameter. In particular the results from Covariance-driven Stochastic Subspace Identification (SSI-Cov) methods are presented.

Keywords: Operational modal analysis; Stabilization diagram; Modal validation criteria; Clustering; Ambient vibration testing; Cable-stayed bridge.

1 Introduction

During the last couple of decades, modal analysis techniques have been widely used in structural health monitoring (SHM) applications. In particular, the operational modal analysis (OMA) has been popularly adopted to analyze the dynamic behavior and damage conditions of full-scale civil structures (Cunha et al. 2013; Koo et al. 2013; Daraemaeker et al. 2008; Siringoringo and Fujino 2008; Ivanovic et al. 2000). Unlike traditional experimental modal analysis methods, OMA techniques are non-disruptive to an operating structure as they utilize ambient excitations originated by the natural sources including the traffic loads, wind and seismic activity. OMA techniques enable the extraction of the modal features of a structure which are typically represented by natural frequencies, damping factors and mode shapes. These modal features are commonly used as important indicators for damage localization, damage-severity determination and tracking the damage evolutions in a structure over time (Doebling et al. 1996; Brownjohn et al. 2005; Abdel Wahab and De Roeck 1999).

Continuous monitoring of a large-scale operating structure is usually critical for studying the changes in modal features and the damage evolution over time. Thus the development of automated OMA algorithms have become a popular research area during the recent years aiming to simplify the modal identification processes and enhance the overall efficiency of modal tracking and damage detection (Rainieri and Fabbrocino 2015; Rainieri and Fabbrocino 2014a; Verboven et al. 2002; Parloo et al. 2002; Rainieri et al. 2011; Bakir 2011).

There have been several past research works focusing on the development of automated OMA algorithms. A method based on the non-parametric frequency domain approaches was reported by Rainieri (2010). This method offers high accuracy in the identification of higher order modes; however, it is not well suited for identifying weakly excited modes. There have also been several research works aiming at developing fully automated OMA algorithms compatible with parametric time-domain methods, in particular, the Stochastic Subspace Identification (SSI) (Reynders et al. 2012; Magalhaes et al. 2009) and the eigen-system Realization Algorithm (ERA) (Zhang et al. 2014). These methods are widely used for vibration-based SHM (Rainieri and Fabbrocino 2015; Magalhaes et al. 2012). The Covariance driven Stochastic Subspace Identification (SSI-Cov) method was applied by Magalhaes et al. (2012) for monitoring the damage conditions of a bridge based on the identified modal characteristics over a 2-year period. The results demonstrate clear relationships between the damage states of the bridge and frequency shifts of the vibration modes.

Both ERA and SSI are expressed based on the state-space model, where the maximum number of modes that can be identified is determined by the selected model order n which governs the size of the state-space matrix (Rainieri and Fabbrocino 2014a). Since the true model order is unknown and inappropriate model order selection can generate biased identification results (Rainieri and Fabbrocino 2014b), the selected model order is normally over-specified to ensure a complete coverage for all the real structural modes. However, spurious mathematical modes are also introduced as a result of this over-specification; thus, stabilization procedure is commonly adopted to identify the physical modes among all the identified modes. In contrast to physical modes, mathematical modes are not identified in a consistent way. The purpose of stabilization is to identify the stable modes with identical modal properties demonstrated through consecutive model orders. (Rainieri and Fabbrocino 2014a).

The stabilization process is usually difficult and complex as it requires several parameters to be manually adjusted. Past automated methods have been successful in eliminating all the spurious modes according to a manually tuned model order n. However, an inappropriate selection of the model order could result in poor modal identification (Rainieri and Fabbrocino 2014b; Ljung 2014). Thus, a critical step towards the development of a fully automated algorithm is the elimination of any manual tuning process associated with the selection of the model order. To address this issue, an improved algorithm for automatically eliminating all mathematical poles is proposed in the present study, which produces accurate results regardless of the model order n selected. The algorithm is developed based on the ideas of clustering approaches for automated OMA by Reynders et al. (2012), along with the following contributions:

1. A novel approach of defining the clustering threshold for hierarchical clustering is proposed. This threshold enables accurate modal identification for any model order n selected.
2. The approach works with any parametric system identification algorithm that uses the system order n as the sole parameter. In particular, the results from Covariance-driven Stochastic Subspace Identification (SSI-Cov) method is presented (Rainieri and Fabbrocino 2014a).

3. Finally, the performance and benefits of the approach for automated modal identification is demonstrated through extensive investigations on a cable-stayed bridge.

The structure of this paper is as follows. In Section 2, a brief background for the SSI-Cov method is provided. In Section 3, the proposed automated OMA algorithm is explained in detail. In Section 4, a detailed description of the cable-stayed bridge structure studied in the paper is provided. Finally, the OMA identification results of the cable-stayed bridge structure and a detailed discussion on the implications of the results are presented in Section 5.

2 Operational Modal Analysis

The discrete-time representation of the equation of motion for a linear time-invariant dynamic system can be given by the state-space formulation as (He and Fu 2001; Ewins 2000; Reynders and De Roeck 2008):

$$\begin{aligned} z(k+1) &= \boldsymbol{A}z(k) + w(k) \\ u(k) &= \boldsymbol{C}z(k) + v(k) \end{aligned} \qquad (1)$$

where $\boldsymbol{A} \in \mathcal{R}^{n\times n}$ is the discrete-time state-space matrix, $z \in \mathcal{R}^{n}$ is the state vector, $w \in \mathcal{R}^{n}$ is the external input assumed to be a white Gaussian noise process, $u \in \mathcal{R}^{l}$ is the vector of measured responses, $\boldsymbol{C} \in \mathcal{R}^{l\times n}$ is the output matrix and $v \in \mathcal{R}^{l}$ is another white noise vector process representing the noise content of the measurements. k indicates the generic time step.

This equation describes an output-only dynamic system using a stochastic state-space model (Rainieri, C. et al. 2007, Peeters and Roeck, 1999, Hermans and Auweraer, 1999). Basically, the idea of OMA is to use output-only or stochastic system identification algorithms, in which the unknown ambient loading conditions are modelled as stochastic quantities with unknown parameters but with known behaviour (for instance, white noise time series with zero mean and unknown covariances). The eigenvalues of the state transition matrix $\boldsymbol{A}$ characterize the dynamic behaviour of a physical system. By computing the state transition matrix $\boldsymbol{A}$ and measurement matrix $\boldsymbol{C}$, it is possible to obtain the modal parameters of the system. The theoretical problem considered here is the estimation of the modal parameters from a given discrete-time output vector $\{u\}$ which is modelled by a discrete-time stochastic state-space as shown in Eq. (1).

According to (Turner and Pretlove, 1998), for a bridge structure, it is valid to assume that the source of excitation as a result of passing traffic is a white Gaussian process. This can be attributed to the randomness in vehicle configurations i.e. different weights and axle configurations, randomness in arrival times, suspension system and road surface profile.

In this paper, SSI-Cov algorithm is adopted to identify a stochastic state-space model from output-only data. SSI-Cov algorithm is a time-domain parametric algorithm that deals with the stochastic realization problem to fit a state space model to the covariance of the responses driven by ambient excitation. SSI-Cov algorithm consists of the following steps (Rainieri and Fabbrocino 2014a): (1) computation of output covariance, $\widehat{\boldsymbol{R}}_{\boldsymbol{i}}$, (2) construction of the block Toeplitz matrix, $\boldsymbol{T}_{\boldsymbol{1}|\boldsymbol{i}}$, (3) decomposition of the Toeplitz matrix, (4) estimation of the controllability and observability matrices and (5) extraction of the modal parameters. These steps are elaborated below.

Let $\boldsymbol{Y}$, an $L \times Q$ matrix be the ambient vibration measurements for a structure, in which L is the total number of sensors and Q is the number of time steps in each set of sensor measurement as,

$$\boldsymbol{Y} = \begin{bmatrix} y_{1,1} & y_{1,2} & \cdots & y_{1,Q} \\ y_{2,1} & y_{2,2} & \cdots & y_{2,Q} \\ \vdots & \vdots & \vdots & \vdots \\ y_{L,1} & y_{L,2} & \cdots & y_{L,Q} \end{bmatrix} \tag{2}$$

The first step of SSI-Cov algorithm is the computation of output correlations $\widehat{\boldsymbol{R}}_{\boldsymbol{i}}$ according to,

$$\widehat{\boldsymbol{R}}_{\boldsymbol{i}} = \frac{1}{Q-i}\left[\boldsymbol{Y}_{(\boldsymbol{1}:\boldsymbol{Q}-\boldsymbol{i})}\right]\left[\boldsymbol{Y}_{(\boldsymbol{i}+\boldsymbol{1}:\boldsymbol{Q})}\right]^{\boldsymbol{T}} \tag{3}$$

where $\boldsymbol{Y}_{(\boldsymbol{1}:\boldsymbol{Q}-\boldsymbol{i})}$ is obtained from the matrix $\boldsymbol{Y}$ by removing the last i samples of data and $\boldsymbol{Y}_{(\boldsymbol{i}+\boldsymbol{1}:\boldsymbol{Q})}$ is obtained by removing the first i samples of data. The parameter i represents the time lag and it is required to be defined by the user. The calculated output correlations at different time lags are then combined to form a block Toeplitz matrix $\boldsymbol{T}_{\boldsymbol{1}|\boldsymbol{i}} \in \mathcal{R}^{Li \times Li}$ as,

$$\boldsymbol{T}_{\mathbf{1}|\boldsymbol{i}} = \begin{bmatrix} \widehat{\boldsymbol{R}}_{\boldsymbol{i}} & \widehat{\boldsymbol{R}}_{\boldsymbol{i}-\mathbf{1}} & \cdots & \widehat{\boldsymbol{R}}_{\mathbf{1}} \\ \widehat{\boldsymbol{R}}_{\boldsymbol{i}+\mathbf{1}} & \widehat{\boldsymbol{R}}_{\boldsymbol{i}} & \cdots & \widehat{\boldsymbol{R}}_{\mathbf{2}} \\ \vdots & \vdots & \vdots & \vdots \\ \widehat{\boldsymbol{R}}_{\mathbf{2}\boldsymbol{i}-\mathbf{1}} & \widehat{\boldsymbol{R}}_{\mathbf{2}\boldsymbol{i}-\mathbf{2}} & \cdots & \widehat{\boldsymbol{R}}_{\boldsymbol{i}} \end{bmatrix} \tag{4}$$

The block Toeplitz matrix $\boldsymbol{T}_{\mathbf{1}|\boldsymbol{i}}$ is decomposed via singular value decomposition as,

$$\left[\boldsymbol{T}_{\mathbf{1}|\boldsymbol{i}}\right] = U\Sigma V^T \tag{5}$$

where $U \in \mathcal{R}^{Li\times Li}$ and $V \in \mathcal{R}^{Li\times Li}$ are orthonormal matrices and $\Sigma \in \mathcal{R}^{Li\times Li}$ is a diagonal matrix containing the positive singular values in descending order. Let n be the number of none zero singular values of $\boldsymbol{T}_{\mathbf{1}|\boldsymbol{i}}$ which indicates the rank of Toeplitz matrix. The observability matrix $O_i \in \mathcal{R}^{Li\times n}$ and the controllability matrix $\Gamma_i \in \mathcal{R}^{n\times Li}$ can be defined as follows:

$$[O_i] = [U_1][\Sigma_1]^{\frac{1}{2}} \tag{6}$$

$$[\Gamma_i] = [\Sigma_1]^{\frac{1}{2}}[V_1]^T$$

where $U_1 \in \mathcal{R}^{Li\times n}$, $\Sigma_1 \in \mathcal{R}^{n\times n}$ and $V_1 \in \mathcal{R}^{Li\times n}$ are obtained by eliminating the zero singular values and the corresponding singular vectors.

The solution of the identification problem can be then obtained by,

$$[\boldsymbol{A}] = [\Sigma_1]^{-\frac{1}{2}}\,[U_1]^T\left[T_{2|i}\right][V_1]\,[\Sigma_1]^{-\frac{1}{2}} \tag{7}$$

$$[\boldsymbol{C}] = O_i(1{:}L) \tag{8}$$

where $\boldsymbol{T}_{\mathbf{2}|\boldsymbol{i}}$ is composed of covariances from lag 2 to $2i$ as,

$$[T_{2|i+1}] = \begin{bmatrix} [\hat{R}_{i+1}] & [\hat{R}_{i}] & \cdots & [\hat{R}_{2}] \\ [\hat{R}_{i+2}] & [\hat{R}_{i+1}] & \cdots & [\hat{R}_{3}] \\ \vdots & \vdots & \vdots & \vdots \\ [\hat{R}_{2i}] & [\hat{R}_{2i-1}] & \cdots & [\hat{R}_{i+1}] \end{bmatrix} \tag{9}$$

At this point the identification problem is theoretically solved. The modal parameters of the system can be extracted from the identified system description $[\boldsymbol{A}]$ and $[\boldsymbol{C}]$ as,

$$[\Psi]^{-1}[\boldsymbol{A}][\Psi] = [Z] \tag{10}$$

$$\lambda_r = \ln(Z_r)\,/\Delta t \tag{11}$$

$$\omega_r = \sqrt{(\lambda_r{}^{R})^2 + (\lambda_r{}^{I})^2}/2\pi \tag{12}$$

$$[\phi] = [\boldsymbol{C}] \times [\Psi] \tag{13}$$

$$\xi_r = \frac{\left|\lambda_r{}^{R}\right|}{\sqrt{\left(\lambda_r{}^{R}\right)^2 + \left(\lambda_r{}^{I}\right)^2}} \tag{14}$$

where Δt is the time step and Z_r is the r-th component of the matrix $[Z]$. $\lambda_r{}^{R}$ and $\lambda_r{}^{I}$ are, respectively, the real and imaginary components of λ_r. ξ_r is the damping factor for the r-th mode and $[\phi]$ is the matrix of mode shapes.

3 Automated Algorithm for Stabilization Process

As previously mentioned since SSI-Cov algorithm is established based on the state-space model, the number of modes to be identified is determined by the model order *n* that is the size of the state-space matrices. Since the automated algorithm is aimed to work with any model order *n*, a large value of *n* is selected to ensure full identification of all structural modes within a given frequency range. However, this might produce many non-physical spurious modes which are to be detected and eliminated through the stabilization process. The identified poles are summarized in a so-called '*stabilization diagram*' which is a representation of the estimated poles at each system order.

The initial stage of the elimination of spurious modes from stabilization diagram is to look for certain indicators of mathematical modes (Reynders et al. 2012). These indicators are as follows and the poles that meet either of these criteria are immediately eliminated.

1. The damping ratio of a mode is not within the range of 0% to 10%. Negative damping ratios and high damping ratios suggest the mode is certainly non-physical.
2. The mode does not have a complex conjugate pair. All physical modes of a structure ought to correspond to another mode where a complex conjugate pair could be formed.
3. The frequency of the mode is not between zero and half of the sampling frequency f_s of the measurement.

3.1 *Modal Validation Criteria*

The next step of the automated OMA is to further eliminate the modes which are undoubtedly spurious using a k-means clustering. Every mode in the stabilization diagram is assigned a characteristic feature vector including five distinctive validation criteria defined in Sections 3.1.1 to 3.1.5. The clustering is established on the basis of these modal validation criteria in order to group the poles to two sets of probably physical modes and certainly mathematical modes.

3.1.1 Distance Measure for Frequencies

The dimensionless distance between undamped eigen-frequencies f_j and f_k of modes j and k:

$$d_f = d(f_j, f_k) = \frac{|f_j - f_k|}{\max(|f_j|, |f_k|)} \quad (15)$$

3.1.2 Distance Measure for Damping Ratio

The dimensionless distance between the damping ratios ξ_j and ξ_k of modes j and k:

$$d_\xi = d(\xi_j, \xi_k) = \frac{|\xi_j - \xi_k|}{\max(|\xi_j|, |\xi_k|)} \tag{16}$$

3.1.3 Modal Assurance Criteria

The Modal Assurance Criteria (MAC) compares the similarity between the unscaled mode shapes ϕ_j and ϕ_k of modes j and k as:

$$MAC(\phi_j, \phi_k) = \frac{\left|\{\phi_j\}^H\{\phi_k\}\right|^2}{\left(\{\phi_j\}^H\{\phi_j\}\right)(\{\phi_k\}^H\{\phi_k\})} \tag{17}$$

where, $\{\phi_j\}^H$ denotes the Hermitian of $\{\phi_j\}$. The value of $MAC(\phi_j, \phi_k)$ lies between 0 and 1 where 1 indicates the maximum similarity.

The functionality of the first three criteria, d_f, d_ξ and MAC are based on the fact that if a mode is a real physical mode, there should be a similar mode with nearly identical modal properties at other system orders. Hence, these three criteria aim to provide a measure of similarity between two modes, one from the current model order, mode j, and the other from the nearest neighbor from the next higher order, mode k. If a similar mode is found at the next higher order, chances are high that the mode at hand is a physical mode. The nearest neighbor is identified based on the mutual distance measured between mode j at model order m and every other mode in the stabilization diagram at model order $m + 2$ according to, (Reynders et al. 2012; Magalhaes et al. 2009):

$$d(j, k) = d(f_j, f_k) + 1 - MAC(\phi_j, \phi_k) \tag{18}$$

The mode k at model order $m + 2$ which has the smallest mutual distance to the mode j is taken as the nearest neighbor to mode j.

Besides the above three criteria, single mode criterion can be defined based on the strength and the complexity of each mode. In a lightly damped structures such as bridges, it is expected that a real physical mode has less complexity and acceptable energy level. On this basis, two more single-mode criteria is considered in the feature vector as follows.

3.1.4 Modal Phase Collinearity

The complexity of a single mode is investigated by the Modal Phase Collinearity (MPC) (Rainieri and Fabbrocino, 2014a; Pappa et al. 1993). The MPC determines the linear relationship between the real (*Re*) part and the imaginary (*Im*) part of the mode shape vector ϕ_j for mode *j* as:

$$MPC_j = \frac{\left\|Re(\{\tilde{\phi}_j\})\right\|^2 + \left(Re\left(\{\tilde{\phi}_j\}^T\right)Im(\{\tilde{\phi}_j\})\right)(2(\varepsilon_{MPC}^2+1)sin^2(\theta_{MPC})-1)/\varepsilon_{MPC}}{\left\|Re(\{\tilde{\phi}_j\})\right\|^2 + \left\|Im(\{\tilde{\phi}_j\})\right\|^2} \tag{19}$$

The q^{th} component of $\{\tilde{\phi}_j\}$ is given by:

$$\tilde{\phi}_{q,j} = \phi_{q,j} - \frac{\sum_{q=1}^{l}\phi_{q,j}}{l} \quad , \qquad q = 1, \dots, l \tag{20}$$

ε_{MPC} and θ_{MPC} are given by:

$$\varepsilon_{MPC} = \frac{\left\|Im(\{\tilde{\phi}_j\})\right\|^2 - \left\|Re(\{\tilde{\phi}_j\})\right\|^2}{2\left(Re\left(\{\tilde{\phi}_j\}^T\right)Im(\{\tilde{\phi}_j\})\right)} \tag{21}$$

$$\theta_{MPC} = \arctan\left(|\varepsilon_{MPC}| + \mathrm{sgn}(\varepsilon_{MPC})\sqrt{1+\varepsilon_{MPC}^2}\right) \tag{22}$$

A MPC value close to 1 indicates a real mode whereas a value of 0 represents a spurious mode.

3.1.5 *Modal Energy Level*

Modal energy level (MEL) is the fifth parameter introduced to indicate the energy contribution of each mode, so as to indicate the real vibration mode and remove spurious modes. It can be defined as (Zhang et al. 2014):

$$MEL_j = \max\left(\sigma\left(\int_0^{f_s/2} C\Psi_r(\exp(jw\Delta t) - \lambda_j)^{-1}\Psi_r{}^{-1}B\Delta t dw\right)\right) \tag{23}$$

where, $\sigma(\cdot)$ denotes a set of singular values, f_s is the sampling frequency, B and C are the input and output matrices, respectively, and Ψ_r is the r^{th} column of Ψ. Ψ is determined from the eigenvalue decomposition of the matrix A. A mode is considered as a real mode if the normalized MEL is close to 1.

3.2 *k-means Clustering*

A distinctive 5-dimensional feature vector is established for each identified pole as, C_X. A k-means clustering is applied to classify the modes into two groups of possibly physical and certainly mathematical spurious modes. The number of clusters (two) is therefore known in advance. Table 1 indicates the ideal values of the modal validation criteria for real and spurious modes.

The centroids of the physical and spurious mode clusters are, respectively, initialized as $C_R = [0,0,1,1,1]$ and $C_S = [1,1,0,0,0]$. The Euclidean distance between each mode at location C_X on the stabilization diagram and the centroids are computed. The mode is then allocated to the group with a smaller distance. The centroids are then relocated by minimizing the objective function as:

$$\{C_R, C_S\} = \text{args}\min_{C_K} \sum_{K=1}^{2} \sum_{X=1}^{n_K} \|C_X - C_K\| \tag{24}$$

where K represents the number of modes in each cluster. This process is iteratively updated until the objective function in Eq. (24) is minimized. The modes are finally categorized into two clusters. The cluster with a centroid C_S is discarded from the stabilization process.

3.3 *Automated Identification Process*

In the previous step, a k-means clustering algorithm was applied to separate the mode candidates into probably physical and certainly mathematical modes. The aim of this step is to cluster the remaining probably physical modes into homogeneous sets that correspond to the same structural modes. The challenge is that the number of structural modes is not known beforehand in the vast majority of cases. Therefore, a hierarchical clustering technique, which is a suitable approach for cases where the number of clusters is not known, is adopted. In hierarchical clustering, each identified mode is linked based on the similarities in specific attributes such as natural frequency and mode shape. The core concept of the automated algorithm with hierarchical clustering is that an automatic threshold is defined so that modes belong to the same set are separated into individual clusters and thus identified. There have been prior applications of hierarchical clustering on OMA with the SSI-Cov method where the algorithm has been demonstrated to be efficient and effective in automatic modal identification (Reynders et al. 2012; Magalhaes et al. 2009). The technique utilized in this work is as follows.

First, each observation (pole) is taken as an individual cluster. The mutual distance between each cluster and all other clusters are calculated according to Eq. (18) and the two clusters with the closest mutual distance are grouped into a new cluster. The mutual distances between every two clusters are then re-computed and this procedure is repeated until the mutual distance between the two closest clusters is greater than a threshold value d_H. This threshold can be understood as the distance up to which modes from different orders are considered to belong to the same physical mode.

Previous works suggested a d_H value based on the mean and standard deviations of the probably physical mode distances as (Reynders et al. 2012; Rubén and Joaquín 2015):

$$d_H = \mu_{C_R} + 2\sigma_{C_R} \tag{25}$$

where the μ_{C_R} and σ_{C_R} are the sample mean and sample standard deviation, respectively, of the mutual distance values. The mutual distances are calculated based on the values of undamped eigen-frequency and MAC assigned to each mode in the final cluster C_R from the previous k-means clustering stage.

In this study, a novel approach to identify d_H, is proposed. At each model order m, the mutual distance between every two poles is calculated and the minimum distance is determined. The threshold value d_H is selected as the median value of the minimum distances obtained for all the model orders. The median value is capable of more effectively eliminating the impact of outliers. This threshold is demonstrated to be capable of generating robust results regardless of the model order n selected and is considered as one of the contributions of the presented work.

Since a real structural mode, theoretically, emerges as a stable pole at different model orders, only the clusters with a high number of modes are real mode clusters, and the other clusters with low number of modes should be ignored. To automate this process, another k-means clustering algorithm with $k = 2$ clusters is applied. The centroid C_R is selected as the number of modes in the largest cluster and $C_S = 0$. To account for the case that all clusters identified from the hierarchical clustering stage represent real mode, a number of additional empty sets are added. This number is equal to the number of clusters with more than one fifth of the number of modes in the largest set; this will avoid any real structural mode to be discarded accidently in the clustering stage (Reynders et al. 2012).

As a result, the final clusters calculated by the k-means method with the centroid closer to C_R will contain all the real vibration modes of the structure. Finally, a demonstrative mode is selected from each cluster utilizing the density-based spatial clustering algorithm (DBSCAN) method (Rubén and Joaquín 2015; Ester et al. 1996; Daszykowski et al. 2002).

Figure 1 illustrates the flowchart of the entire SSI-Cov algorithm adopted in this work.

4 Testing Structure

A short-span cable-stayed bridge over the Great Western Highway in the state of New South Wales, Australia (33°45'50.49"S, 150°44'31.14"E) was considered as a case study to test and validate the performance of the proposed method. Figure 2 shows an illustration of the bridge.

4.1 *Description of Bridge*

The considered cable-stayed bridge has a single A-shaped steel tower with a composite steel-concrete deck. The bridge is composed of 16 stay cables with semi-fan arrangement. The bridge span and the tower height are 46 m and 33 m, respectively. This bridge provides a connection between two Western Sydney University campuses over the Great Western highway and carries one traffic lane and one sidewalk. The deck has a thickness of 0.16 m and a width of 6.3 m and it is supported by four I-beam steel girders. These girders are internally attached by a set of equally-spaced floor beams as depicted in Figure 3.

4.2 *Sensor Array*

The measurement grid for the dynamic test consists of 25 synchronized accelerometers to measure the acceleration responses of the deck, cables and the mast. These sensors were permanently installed on the bridge in order to monitor the dynamic behavior of the bridge and to identify the modal parameters. It is worth noting that during the instrumentation, the traffic lanes in Great Western Highway under the bridge were partially closed; thus, no roving of the sensors were considered due to the access limitations.

24 uni-axial sensors were placed under the deck at the intersection of the girders and floor beams to measure the vertical acceleration of the bridge, (see Figure 4). These sensors are low noise accelerometers with model number 2210-002 manufactured by Silicon Design, Inc (2010). The 2210-002 is a sensor that incorporates a 1210L micro-machined capacitive accelerometer. This model can detect accelerations within the range of ± 2 g with an output noise of 10 μg/√Hz and sensitivity of 2,000 mV/g.

The under deck accelerometers were adhered to the lightly sanded and cleaned paint using adhesive tape and covered with elastic joint sealant. All installations were coated with paint to reduce corrosion and improve the visual amenity of the installation. Figure 5 shows one of the sensors mounted under the girder before coating.

Another four 2210-002 uni-axial accelerometers were mounted on the cables on the eastern side of the bridge. These sensors measure the acceleration response of the cables in the vertical plane orthogonal to the line of the stay. In addition, one tri-axial accelerometer (Silicon Designs 2460-002) was installed on top of the mast to measure the vertical, lateral and longitudinal acceleration responses of the tower.

4.3 *Data Acquisition and Measurement Set up*

The signal conditioning and data logging software consist of an embedded PC and HBM Quantum-X data logger to record data. This system provides an integrated and reliable device to log high quality data with 24bit resolution with bandwidth capability of 0 to 3 kHz. This hardware combines instrument excitation, voltage regulation, digitization, anti-aliasing filters and data logging. The logging software is Catman. The software collects all channels at a default sample rate of 600 Hz with an anti-aliasing filter. The 3 dB cut-off frequency of the filter is 100 Hz and it is a fourth order Bessel low-pass filter. The selection of this high sampling frequency in the system is solely to meet the requirements of other research activities on this bridge i.e. Bridge-Weigh-in-Motion (BWIM) and tensor analysis. It should be noted that a dense array of strain gauges, timely synchronized with the accelerometers, have been installed under the deck in this bridge which is out of the scope of this paper (Hamed Kalhori et al. 2017).

For the purpose of identifying the modal properties of the bridge under operational conditions and consequently building time histories of modal parameters, the dynamic monitoring system continuously records the vibration response of the bridge and it produces a file with acceleration time series per 10 minutes. A total number of 144 files is generated per day. 360,000 samples are acquired for each channel for a 10-minute-long acceleration signal. The measured data are continuously transferred over a 4G cellular network to the database.

Figure 6 (a) illustrates typical acceleration time signal obtained from a 10-minute file from channel A7. Light traffic flow over the bridge is evident from this figure. Typical ambient part of the response, once no vehicle is traveling over the bridge i.e. the first 16.67 seconds (≈ 0.3 min) is illustrated in Figure 6 (b). As seen, the vibration of the bridge with its first natural frequency is quite obvious in the acceleration response.

22 days of monitoring data, continuously acquired from the 1st of November until the 22nd of November 2016 are used in this paper for the purpose of the operational modal analysis. This selection was only made due to the availability of the data in this time period. For each day, three files were considered. The files were selected from different times within 24 hours including midnight, and rush traffic hours. This provides a total number of 66 10-minute-files for our investigations.

4.4 *Preprocessing and Parameters of the Algorithm*

The analysis of the experimental data involves initial pre-processing operations to eliminate the offset and to ensure there is no spike or unreasonable noise in the signals. The entire 10-minute acceleration response was adopted for the analysis. This includes 360,000 data points from each channel. A Hanning window was applied to the time signals to minimize leakage. Parameter i, was selected to be 100 and a maximum model order of 160 was considered to construct the stabilization diagram.

In a separate study, the time signals were decimated with a factor of 5 which resulted in 72,000 samples from each channel. Decimation of the signals can help to enhance the ability of the estimation process in identification of the lower frequency modes. However, it was realized that the results with and without decimation are quite similar, hence, the results obtained from the original time signals were only presented.

5 Operational Modal Analysis Results

The collected responses from all 24 accelerometers installed under the deck of the bridge are used to study the vibration characteristics of the bridge. The operational modal analysis adopting SSI-Cov algorithm is performed on the previously elaborated datasets including 66 files, which each of them is a 10-min acceleration response from the bridge.

Table 2 summarizes the identification results within the frequency range of [0-13 Hz]. As seen, within this frequency range, nine modes have been extracted including two closely-spaced modes around 3.5 Hz. It was realized that not all of the modes are extracted from every single dataset. The last column of Table 2 specifies the percentage of identification for each particular mode amongst 66 datasets. As shown, the first mode has been identified from all of the 66 datasets, however, the ninth mode have been identified only from 76% of datasets i.e. 50 datasets. A detailed discussion explaining the missed identification of some modes can be found in Section 5.2.

ω_{mean} shows the mean value of the natural frequency for each mode obtained from 66 datasets and ω_{RSD} shows the relative standard deviation (RSD) for the identified natural frequencies; RSD is a standardized measure obtained by normalizing the standard deviation with respect to the mean value and it shows the dispersion of a distribution. A relative standard deviation of 1% to 2% is observed for the identified eigen-frequencies which is quite low and indicates the consistency of the modal identification over time. ξ_{mean} and ξ_{RSD}, respectively, show the mean damping ratio for each mode and the corresponding relative standard deviation. As illustrated in Table 2, the uncertainty on the damping ratio estimates is much higher than the uncertainty obtained for the natural frequencies and greater discrepancies are observed in damping estimation. Past research works (Magalhaes et al. 2009; Geothals et al. 2004) have also had similar observations and the explanation for this is that large scattering and dispersion are common for the damping ratios estimated from OMA methods. Rainieri et al. (2010) suggested that the presence of inherent limitations or inaccuracies of data processing methodologies can both lead towards high variations in damping ratio estimates. Inappropriate selection of the model order for the stabilization diagram may also enlarge the scattering of damping ratio for each identified mode. The high uncertainty in the identification of damping in civil structures can also be attributed to the fact that damping is strongly influenced by the magnitude of the dynamic response of a structure (Reynders et al. 2008).

Figure 7 illustrates the boxplot of the nine identified modes. Based on this figure, higher modes are experiencing higher standard deviation compared to the lower modes. Figure 8 shows the first nine mode shapes of the structure. Mode shape estimates were constructed using only the data locations corresponded to the measuring points in the testing and also zero deflection boundaries at supports. In the plan view presentation of each mode shape, an interpolating function is applied to provide a shaded approximation of the continuous mode shape. As seen in Figure 8, the reconstructed mode shapes encompass bending and torsional modes of the deck. Mode 1 is the first vertical bending mode of the deck which was consistently identified from all 66 datasets. Modes 2 and 3 make up a double mode which corresponds to the second vertical bending mode. Mode 4 corresponds to the third bending mode and modes 5 and 6 show a mixture of torsion and bending. The last three modes is a combination of the fourth bending mode and torsion.

5.1 *Consistency of Mode Shapes over Time*

For any modal identification process, it is quite important to ensure the consistency of the mode shapes over time. MAC can be used for this purpose to quantify the correlation between the modes measured during different tests. MAC makes use of the orthogonality properties of the mode shapes to compare modes from different tests. If the modes are identical, a scalar value of one is calculated, otherwise it would be very small close to 0. The utilization of MAC can help for mode pairing to track a particular mode from different datasets and to see the consistency of identification of a particular mode between different datasets. For two arbitrary datasets, the MAC matrix was generated and it was illustrated in Figure 9. Basically, the horizontal axis shows the nine modes identified from a particular dataset and the vertical axis shows the identification results from a separate dataset. As seen, the diagonal MAC values are very high (>0.9) which shows the fact that the identified nine modes from two datasets are very similar and highly correlated. In general, very small MAC numbers are observed for off-diagonal members which is expected due to the orthogonality of the mode shapes. However, the closely-spaced modes 2 and 3 show some coupling through the off-diagonal MAC values. These results generally outline a very good agreement between the identified modes from different datasets. Similar graphs were obtained from different datasets and because of space restriction only one graph was presented.

5.2 *Missed Identification*

As discussed earlier, not all of the modes can be extracted from all 66 datasets. To further investigate the missed identification of some modes, the acceleration responses of the bridge (10 minutes) for two different cases were compared with each other: a case where only one mode, which is the first mode, has been identified, and a case that all of the nine modes have been identified. Figure 10 (a) illustrates the acceleration response obtained from channel A7 for a case that all modes have been extracted whereas Figure 10 (b) shows the response for a case that only the first mode has been identified and no identification of the other eight modes has been achieved. From this figure, it is quite obvious that the level of response is almost 25 times higher in Figure 10 (a) compared to the response presented in Figure 10 (b) which coincides with the time windows of these two files, i.e. mid-day versus mid-night. It demonstrates the fact that if the ambient excitation on the bridge is not adequate enough, there is a high chance that the modes, in particular the higher modes, are not excited. To fully address the issue of missing modes, a separate study was conducted. This time, the vibration response of the bridge was collected from two different days: a working day and a weekend. Each day provides 24 hr×6 files/hr=144 10-minute files. It should be noted that the previously elaborated datasets including 66 files from 22 days of monitoring in November 2016 are the main datasets which have been adopted for our investigations in this paper and the continuous 24 hour data from these two days i.e. one weekday and one weekend has been solely adopted to further validate the impact of ambient excitation on missing modes and no further data analysis has been done using these datasets).

For each file, (in total, 144 files per day) the first singular value of SVD (Singular Value Decomposition) of spectral density matrix was calculated. This provides an estimation of the auto spectral density of the system in modal coordinates and the peak in the SVD curve is expected to represent a structural mode. Figure 10 (a) and (b), respectively, show the spectrograms of the response combining all of the 144 files from 24 hours for a weekday and for a weekend. The horizontal axis in these figures is frequency and the vertical axis is the time within 24 hours. The starting time in the vertical axis is almost 11:00 am. The color reflects the strength of the frequency component, i.e. the lighter the shade is, the higher the strength of the frequency component is. From this figure, it is quite evident that the first mode has been well excited at any time within the 24 hours during weekday and weekend. This figure also implies that modal identification process fails to extract the modes while there is not enough traffic on the bridge i.e. the time window between 8:00 pm to 6:00 am. It can also be observed that within the time window of 6:00 am to 8:00 pm the identification process has been more successful on weekday rather than weekend, again due to sufficiency of excitation on the bridge as a result of passing traffic. Additional piece of information that can be captured from this figure is that there is frequency variation in the modal frequencies which can be related to the environmental changes within 24 hours. From these investigations it appears that while the excitation level during ambient vibration is insufficient to produce reasonably strong vibration, the estimation process more likely fails to extract all of the modes particularly the higher modes.

5.3 *Effectiveness of the Newly Proposed Hierarchical Clustering Threshold*

As mentioned earlier, one of the main contributions of the current work is to define a novel way of automatically defining the hierarchical clustering threshold, d_H to enable the accurate identification of a complete set of modal parameters, regardless of the system order chosen. In order to demonstrate the superiority of this new threshold over the previous threshold (old threshold) (see Eq. 25), the following investigation was carried out.

For a typical 10-minute acceleration response collected from the bridge, shown in Figure 12, the SSI-Cov technique was applied. Five different system orders ranging from 160 to 200 with an increment of 10 were considered. Both the new and the old thresholds were adopted and the results were compared. Table 3 and Table 4, respectively, summarize the identified modes using the old and the new thresholds. As seen, the old threshold can only provide successful identification of the modes where the system order is 160 and it fails to identify the modes for the other system orders, i.e. 170, 180, 190 and 200. However, by using the new threshold all the modes are successfully identified no matter what system order is considered.

Figure 13 illustrates the stabilization diagrams for the system orders 170, 180 and 190. Column (a) is the unfiltered stabilization diagram, column (b) is the filtered stabilization diagram using the old threshold and column (c) is the filtered stabilization diagram using the new threshold. The green vertical lines indicate the stable modes and the blue curve shown in the figures indicates the first singular value of SVD (Singular Value Decomposition) of spectral density matrix at each frequency coordinate.

Consistent to the results presented in Table 3 and Table 4, it is clear that the old threshold fails to identify the modes even at situations that they look stable. In contrast, by utilizing the new threshold, all of the modes even the closely-spaced modes are successfully identified. Please note that in the filtered stabilization diagram using the new threshold, there are two closely-spaced modes around 3.5 Hz (3.597 Hz and 3.643 Hz). System order 200 provides similar result to the one obtained from the system order 190 and because of space restrictions it was not presented. This investigation implies that the procedure of eliminating the spurious modes using the new threshold is effective and as a result, the homogeneous groups of modes which represent the real physical modes are clearly detected.

To further investigate the superiority of the new threshold over the old threshold, the dendrogram of the hierarchical clustering for the system order 170 was studied and the result was shown in Figure 14. The red dotted line and the grey dashed lines, respectively, illustrate the position of the cut-off distances for the hierarchical clustering obtained by the old and the new thresholds. It is clear that the new threshold proposes a much lower threshold (0.0040) than the old threshold (0.1513) for system order 170. As indicated by the identification results, within the frequency range of 0-13Hz, nine structural modes have been successfully identified with the new threshold however no structural mode is identified using the old threshold. These results imply that the old threshold value is too high for the hierarchical clustering. In hierarchical clustering, modes with similar attributes are linked to each other to produce the dendrogram. Ideally, the threshold value signifies that each tree underneath the threshold should represent a single real structural mode. However, because the old threshold is much higher than the desired threshold, distinct modes have been merged into the same cluster. This usually results in one big cluster containing many modes of distinctive frequencies where the total number of the modes in this cluster is much greater than the number of the modes in the other clusters. Consequently, during the next stage of the algorithm where the second *k*-means clustering is applied, based on the number of the modes in each cluster, the largest cluster significantly overweighs the other smaller clusters and thus the smaller clusters are classified as the clusters with spurious modes.

5.4 *Automatic versus Manual OMA*

This section aims to compare the identification results using manual and automatic algorithms. Basically, the manual cleaning of the stabilization diagram is performed based on manually tuning some parameters i.e. the frequency tolerance (t_f), damping ratio tolerance (t_ξ), and MAC value. Obviously, the smaller values of t_f and t_ξ and a larger value of MAC indicate more strict tolerances, resulting in identification of the most dominant modes of the structures. These modes are actually the modes that consistently appear in the stabilization diagram as stable modes. Hence, for the strict tolerances, we are confident that most of the identified modes are real, however, we may potentially miss some real modes because they do not satisfy the defined tolerances.

To investigate the effect of the parameters to be manually tuned for cleaning of the stabilization diagram, sufficiently excited datasets were chosen. Table 5 compares the first nine natural frequencies of the bridge obtained from the manual algorithm for different values of t_f, t_ξ and MAC values with the modes obtained from the automated algorithm. For very strict tolerances ($t_f = 0.001, t_\xi = 0.005$ and MAC=0.99), a few number of modes are identified. However, less strict tolerances result in identification of a larger number of modes, as expected. The tolerance set of t_f, t_ξ and MAC, respectively, equal to 0.010, 0.100, and 0.99 looks suitable as the damping ratio tolerance is neither very small nor very large. This tolerance set leads to identification of the first eight modes. Figures 15 (a) and (b), respectively, show the unfiltered stabilization diagram and the filtered stabilization diagram obtained from the manual SSI-Cov algorithm using this tolerance set. By making the tolerances less strict, additional modes are identified, where the majority of them vary between 20 Hz and 50 Hz. However, chances are high that some of these additional modes are spurious. It should also be noticed that none of tolerance sets in Table 5 resulted in identifying the ninth mode, whereas, this mode is identified by the automated algorithm and is visually identifiable in the unfiltered stabilization diagram as depicted in Figure 15 (a).

As a general conclusion, finding the most appropriate tolerance values is the key factor in the manual algorithm so that as many real modes as possible are identified and, at the same time, no spurious modes are generated. This highlights the importance of the automated parameter tuning and also the superiority of the automatic algorithm.

It is also important to see the consistency of the identification results between the manual and the automated algorithms to make sure that the identified modes are identical. The mode shapes identified by the automated algorithm and the manual algorithm with the tolerance values of 0.010, 0.100, and 0.99, respectively, for t_f, t_ξ and MAC were used for calculation of MAC matrix. The generated MAC matrix is shown in Figure 16. Since, the manual algorithm did not identify the ninth mode, the MAC was computed for the first eight modes. The horizontal axis represents the modes obtained from the automated algorithm and the vertical axis shows the modes identified by the manual algorithm. As seen, the diagonal MAC values are very high (>0.9) representing the high correlation between the modes obtained from the both methods. However, the closely-spaced modes 2 and 3 and modes 6 and 7 show some coupling through the off-diagonal MAC values. In general, this figure highlights the consistency of the identified modes between two methods.

6 Conclusions

In this paper, an automated operational modal analysis algorithm using Covariance-driven Stochastic Subspace Identification (SSI-Cov) method was presented. Based on the ideas of implementing clustering approaches to automatically clear the stabilization diagram, this algorithm incorporates the concept of Mode Energy Level as a new criterion for the initial *k*-means clustering and introduces a novel threshold for the hierarchical clustering process. Accurate and robust modal identification results are obtained when this automated operational modal analysis algorithm is applied to a cable-stayed bridge structure. The superiority of the proposed threshold over the old threshold was validated and it was demonstrated that the new threshold can result in successful modal identification regardless of the system order considered. The method was also proved to provide consistent identification results using nearly one month of data from this bridge. High MAC values (Modal Assurance Criteria) (> 0.9) was observed between the identified modes from different datasets. The issue of missed identification was extensively investigated and it was realized that while the excitation level during ambient vibration is insufficient to produce reasonably strong vibration, the estimation process is more likely to fail to extract all of the modes particularly the higher modes. This automated algorithm is proved to generate results with comparable accuracy to the corresponding results from expertise manual analysis and it is recommended to be used as an operational modal analysis framework for testing the full scale bridge and building structures.

7 Acknowledgments

This project was funded by New South Wales Government in Australia and was undertaken by division Data61 within the Commonwealth Scientific and Industrial Research Organization (CSIRO) in Australia. The authors also wish to express their gratitude to the Western Sydney University for provision of the support and facilities for this research work.

8 References

[1] Abdel Wahab MM, De Roeck G. Damage detection in bridges using modal curvatures: application to a real damage scenario. Journal of Sound and Vibration. 1999; 226: 217-235. DOI: 10.1006/jsvi.1999.2295.

[2] Alamdari, M.M., Li, J., Samali, B., Ahmadian, H. and Naghavi, A., 2013. Nonlinear joint model updating in assembled structures. Journal of Engineering Mechanics, 140(7), p.04014042.

[3] Alamdari, M.M., Li, J. and Samali, B., 2015. Damage identification using 2-D discrete wavelet transform on extended operational mode shapes. Archives of Civil and Mechanical Engineering, 15(3), pp.698-710.

[4] Bakir PG. Automation of the stabilization diagrams for subspace based system identification. Expert Systems with Applications. 2011; 38: 14390-14397. DOI: 10.1016/j.eswa.2011.04.021.

[5] Brownjohn JMW, Moyo P, Omenzetter P, Chakraborty S. Lessons from monitoring the performance of highway bridges. Structural Control and Health Monitoring. 2005; 12:227-244.

[6] Cunha A, Caetano E, Magalhaes F, Moutinho C. Recent perspectives in dynamic testing and monitoring of bridges. Structural Control and Health Monitoring. 2013; 20: 853-877. DOI: 10.1002/stc.1516.

[7] Ester M, Kriegel HP, Sander J, Xu X. A density-based algorithm for discovering clusters in large spatial databases with noise. Proceedings of 2nd international conference on knowledge discovery and data mining; 1996: 226-231.

[8] Farrar CR, James III GH. System identification from ambient vibration measurements on a bridge. Journal of Sound and Vibration. 1997; 205: 1-18. DOI: 10.1006/jsvi.1997.0977.

[9] Daszykowski M, Walczk B, Massart DL. Looking for natural patterns in analytical data. 2. Tracing local density with OPTICS. Journal of Chemical Information and Computer Sciences. 2002; 42: 500-507.

[10] Deraemaeker A, Reynders E, De Roeck G, Kullaa J. Vibration-based structural health monitoring using output-only measurements under changing environment. Mechanical Systems and Signal Processing. 2008; 22: 34-56. DOI: 10.1016/j.ymssp.2007.07.004.

[11] Doebling SW, Farrar CR, Prime MB, Shevitz DW, Damage identification and health monitoring of structural and mechanical systems from changes in their vibration characteristics: a literature review (No. LA-13070-MS). Las Alamos National Laboratory, NM; 1996.

[12] Ewins DJ. Modal testing: theory and practice. England: Research Studies Press Ltd; 2000.

[13] Goethals I, Vanluyten B, De Moor B. Reliable spurious mode rejection using self-learning algorithm. Proceedings of ISMA 2004 International Conference on Noise and Vibration Engineering, Leuven, Belgium, 2004.

[14] HBM. http://www.hbm.com; 2016 [accessed 17.08.2016].

[15] He J, Fu Z. Modal Analysis. Oxford: Butterworth-Heinemann; 2001.

[16] He, X., Moaveni, B., Conte, J.P., Elgamal, A. and Masri, S.F., 2008. Modal Identification Study of Vincent Thomas Bridge Using Simulated Wind‐Induced Ambient Vibration Data. Computer‐Aided Civil and Infrastructure Engineering, 23(5), pp.373-388.

[17] Hermans, L. and Van der Auweraer, H., 1999. Modal testing and analysis of structures under operational conditions: industrial applications. Mechanical systems and signal processing, 13(2), pp.193-216.

[18] Ivanovic SS, Trifunac MD, Todorovska MI, Ambient vibration tests of structures – a review. ISET Journal of Earthquake Technology. 2000; 37: 165-197.

[19] Juang JN, Pappa RS. An eigensystem realization algorithm for modal parameter identification and model reduction. Journal of Guidance Control and Dynamics. 1985; 8: 620-627.

[20] Ljung L. System Identification: Theory for the User. 2nd ed. Upper Saddle River, NJ. Prentice Hall PTR. 2014.

[21] Kalhori, H., Alamdari M.M., Zhu, X., Samali, B., Mustapha, S., Non-intrusive schemes for speed and axle identification in bridge-weigh-in-motion systems. Measurement Science and Technology. 2017; 28 (2), 025102.

[22] Koo KY, Brownjohn JMW, List DI, Cole R. Structural health monitoring of the Tamar suspension bridge. 2013; 20: 609-625. DOI: 10.1002/stc.1481.

[23] Makki Alamdari, M., 2015. Vibration-based structural health monitoring (Doctoral dissertation).

[24] Magalhaes F, Cunha A, Caetano E. Vibration based structural health monitoring of an arch bridge: From automated OMA to damage detection. Mechanical Systems and Signal Processing. 2012; 28: 212-228. DOI: 10.1016/j.ymssp.2011.06.011.

[25] Magalhaes F, Cunha A, Cateno E. Online automatic identification of the modal parameters of a long span arch bridge. Mechanical Systems and Signal Processing. 2009; 23: 316-329. DOI: 10.1016/j.ymssp.2008.05.003.

[26] Pappa RS, Elliott KB, Schenk A. A consistent-mode indicator for the eigensystem realization algorithm. Journal of Guidance Control and Dynamics. 1993; 16: 852-858.

[27] Parloo E, Verboven P, Guillaume P, Van Overmeire M. Autonomous structural health monitoring – part II: vibration-based in-operation damage assessment. Mechanical Systems and Signal Processing. 2002; 16: 659-675. DOI: 10.1006/mssp.2002.1493.

[28] Peeters, B. and De Roeck, G., 1999. Reference-based stochastic subspace identification for output-only modal analysis. Mechanical systems and signal processing, 13(6), pp.855-878.

[29] Rainieri, C., Fabbrocino, G., Cosenza, E. and Manfredi, G., 2007, April. Implementation of OMA procedures using labview: theory and application. In 2nd international operational modal analysis conference (Vol. 30, pp. 1-13). Copenhagen: Denmark.

[30] Rainieri C, Fabbrocino G. Automated output-only dynamic identification of civil engineering structures. Mechanical Systems and Signal Processing. 2010; 24: 678-695

[31] Rainieri C, Fabbrocino G, Cosenza E. Some remarks on experimental estimation of damping for seismic design of civil constructions. Shock and Vibration. 2010; 17: 383-395. DOI: 10.3233/SAV-2010-0534.

[32] Rainieri C, Fabbrocino G, Cosenza E. Near real-time tracking of dynamic properties for standalone structural health monitoring systems. Mechanical Systems and Signal Processing. 2011; 25: 3010-3026. DOI: 10.1016/j.ymssp.2011.04.010.

[33] Rainieri C, Fabbrocino G. Development and validation of an automated operational modal analysis algorithm for vibration-based monitoring and tensile load estimation. Mechanical Systems and Signal Processing. 2015; 60-61: 512-534. DOI: 10.1016/j.ymssp.2015.01.019.

[34] Rainieri C, Fabbrocino G. Operational Modal Analysis of Civil Engineering Structures. New York: Springer; 2014a.

[35] Rainieri C, Fabbrocino G. Influence of model order and number of block rows on accuracy and precision of modal parameter estimates in stochastic subspace identification. International Journal of Lifecycle Performance Engineering. 2014b; 1: 317-334. DOI: 10.1504/IJLCPE.2014.064099.

[36] Reynders E, Houbrechts J, De Roeck G. Fully automated (operational) modal analysis. Mechanical Systems and Signal Processing. 2012; 29: 228-250. DOI: 10.1016/j.ymssp.2012.01.007.

[37] Reynders E, De Roeck G. Reference-based combined deterministic-stochastic identification for experimental and operational modal analysis. Mechanical Systems and Signal Processing. 2008; 22: 617-637. DOI: 10.1016/j.ymssp.2007.09.004.

[38] Rubén BK, Joaquín BN. Evaluation of an automatic selection methodology of model parameters from stability diagrams on a damage building. Dynamics of Civil Structure, Volume 2: Proceedings of the 33rd IMAC, A conference and Exposition on Structural Dynamics; 2015: 545-552.

[39] Silicon Designs Advanced Accelerometers. High-Accuracy Industrial-Grade MEMS Capacitive Accelerometers. http://www.silicondesigns.com/; 2016 [accessed 14.08.2016].

[40] Siringoringo DM, Fujino Y. System identification of suspension bridge from ambient vibration response. Engineering Structures. 2008; 30: 462-477. DOI: 10.1016/j.engstruct.2007.03.004.

[41] Turner, J.D. and Pretlove, A.J., 1988. A study of the spectrum of traffic-induced bridge vibration. Journal of Sound and Vibration, 122(1), pp.31-42.

[42] Verboven P, Parloo E, Guillaume P, Van Overmeire M. Autonomous structural health monitoring – part I: modal parameter estimation and tracking. Mechanical Systems and Signal Processing. 2002; 16: 637-657. DOI: 10.1006/mssp.2002.1492.

[43] Zhang G, Ma J, Chen Z, Wang R. Automated eigensystem realisation algorithm for operational modal analysis. Journal of Sound and Vibration. 2014; 333: 3550-3563.

Table 1. The ideal values of the modal validation criteria for real and spurious modes.

No.	Criterion	Physical Mode	Spurious Mode
1	$d(f_j, f_k)$	0	1
2	$d(\xi_j, \xi_k)$	0	1
3	$MAC(\boldsymbol{\phi_j}, \boldsymbol{\phi_k})$	1	0
4	MPC_j	1	0
5	MEL_j	1	0

Table 2. Modal identification results from 22 days of monitoring in November 2016.

Mode number	ω_{mean}	ω_{RSD} (%)	ξ_{mean} (%)	ξ_{RSD} (%)	Identified modes
1	2.032	0.98	0.9	42.23	100%
2	3.548	1.66	2.5	60.00	85%
3	3.649	1.15	2.2	63.14	81%
4	5.584	1.45	1.9	57.89	67%
5	6.136	2.33	2.8	42.85	82%
6	8.044	1.71	1.7	52.94	73%
7	8.671	2.09	1.7	70.58	60%
8	11.561	1.89	1.8	27.77	64%
9	12.31	1.46	1.4	42.86	76%

Table 3. Identification results using the old threshold.

System Order	ω_1	ω_2	ω_3	ω_4	ω_5	ω_6	ω_7	ω_8	ω_9
160	2.017	3.570	3.643	5.569	6.046	8.257	8.739	11.309	12.172
170	---	---	---	---	---	---	---	---	---
180	2.017	3.597	---	---	---	---	8.739	11.309	---
190	---	---	---	---	---	---	---	11.305	---
200	---	---	---	---	---	---	---	11.305	---

Table 4. Identification results using the new threshold.

System Order	ω_1	ω_2	ω_3	ω_4	ω_5	ω_6	ω_7	ω_8	ω_9
160	2.017	3.597	3.643	5.568	6.044	8.255	8.739	11.309	12.176
170	2.017	3.597	3.643	5.568	6.051	8.255	8.740	11.309	12.176
180	2.017	3.597	3.643	5.568	6.051	8.255	8.740	11.307	12.176
190	2.017	3.597	3.643	5.568	6.051	8.255	8.739	11.307	12.176
200	2.017	3.597	3.643	5.568	6.051	8.255	8.740	11.305	12.177

Table 5. Natural frequencies obtained from the automated SSI-Cov algorithm and the manual SSI-Cov algorithm for different values of frequency tolerance (t_f), damping ratio tolerance (t_ξ), and MAC.

Manual algorithm

Manual parameters t_ξ, t_f, MAC	ω_1	ω_2	ω_3	ω_4	ω_5	ω_6	ω_7	ω_8	ω_9
0.005, 0.001, 0.99	2.017	3.597	3.643	---	---	---	8.740	---	---
0.008, 0.002, 0.99	2.017	3.597	3.643	---	---	8.255	8.739	---	---
0.010, 0.007, 0.99	2.017	3.597	3.643	---	6.044	8.262	8.747	---	---
0.050, 0.010, 0.99	2.017	3.596	3.644	---	6.044	8.262	8.740	11.303	---
0.100, 0.001, 0.99	2.017	3.596	3.644	---	6.044	8.255	8.747	11.304	---
0.100, 0.010, 0.99	2.017	3.596	3.643	5.568	6.044	8.258	8.747	11.293	---
0.100, 0.010, 0.95	2.017	3.596	3.643	5.568	6.044	8.258	8.747	11.293	---
0.100, 0.500, 0.95	2.017	3.596	3.643	5.568	6.044	8.258	8.747	11.293	---
0.500, 0.010, 0.95	2.017	3.596	3.643	5.579	6.044	8.258	8.747	11.293	---
0.800, 0.500, 0.95	2.017	3.596	3.643	5.561	6.044	8.258	8.747	11.291	---

Automated algorithm

ω_1	ω_2	ω_3	ω_4	ω_5	ω_6	ω_7	ω_8	ω_9
2.017	3.597	3.643	5.568	6.044	8.255	8.739	11.309	12.176

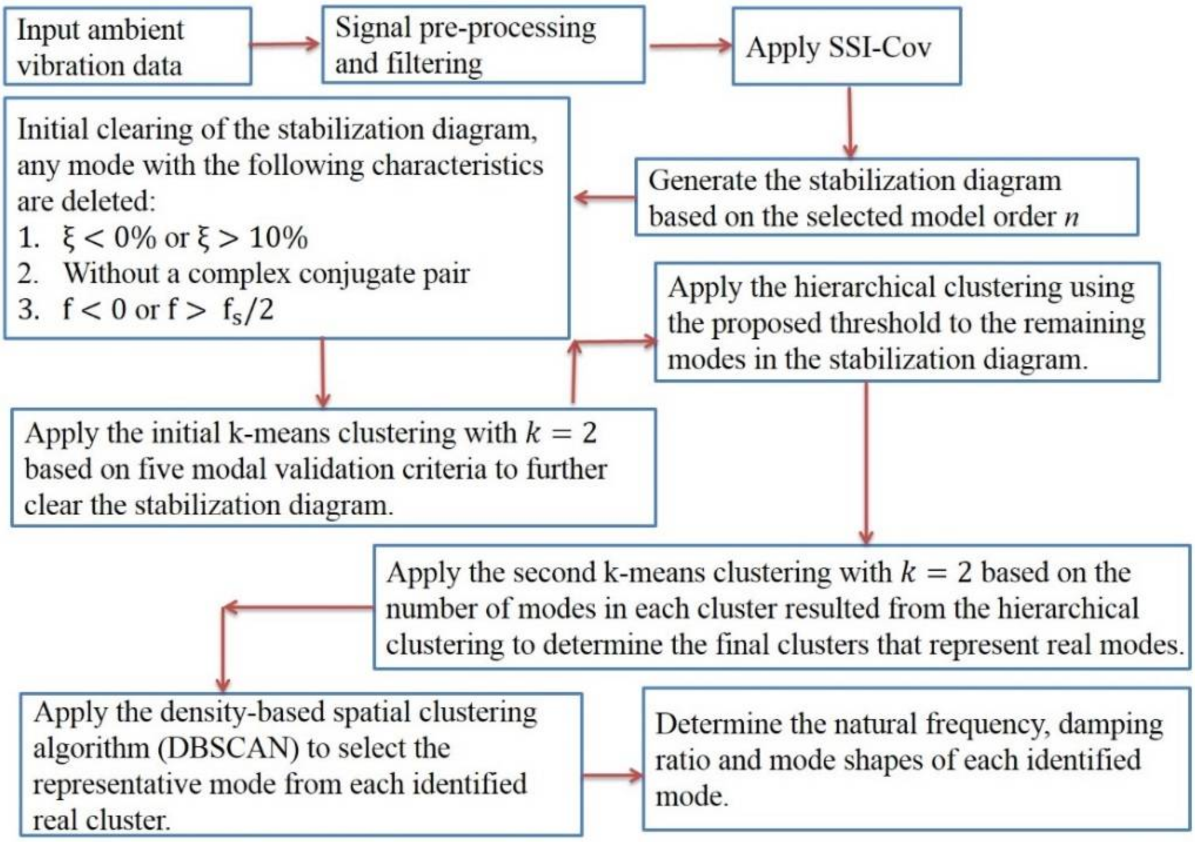
Input ambient vibration data
Signal pre-processing and filtering
Apply SSI-Cov
Generate the stabilization diagram based on the selected model order n
Initial clearing of the stabilization diagram, any mode with the following characteristics are deleted:
1. $\xi < 0\%$ or $\xi > 10\%$
2. Without a complex conjugate pair
3. $f < 0$ or $f > f_s/2$
Apply the initial k-means clustering with $k = 2$ based on five modal validation criteria to further clear the stabilization diagram.
Apply the hierarchical clustering using the proposed threshold to the remaining modes in the stabilization diagram.
Apply the second k-means clustering with $k = 2$ based on the number of modes in each cluster resulted from the hierarchical clustering to determine the final clusters that represent real modes.
Apply the density-based spatial clustering algorithm (DBSCAN) to select the representative mode from each identified real cluster.
Determine the natural frequency, damping ratio and mode shapes of each identified mode.

(a) (b)

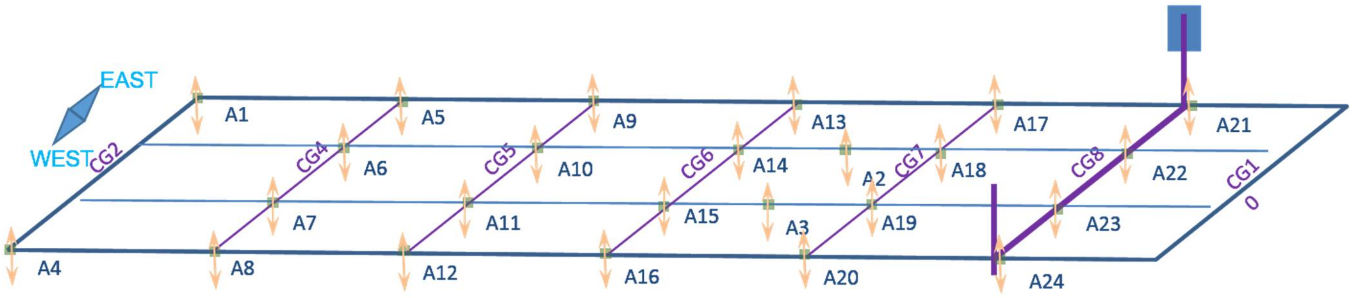
EAST
WEST
CG2
CG4
CG5
CG6
CG7
CG8
CG1
0
A1
A5
A9
A13
A17
A21
A6
A10
A14
A2
A18
A22
A7
A11
A15
A3
A19
A23
A4
A8
A12
A16
A20
A24

Figure

Click here to download Figure Figure 5.tif

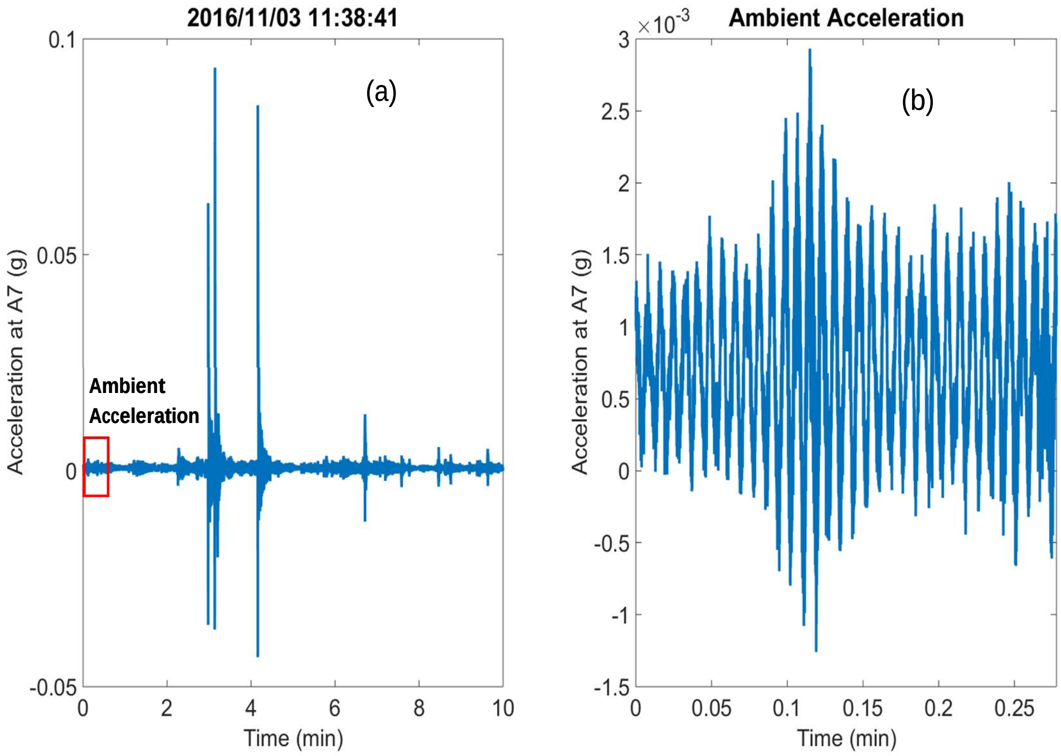
2016/11/03 11:38:41
(a)
Acceleration at A7 (g)
Ambient
Acceleration
Time (min)
0.1
0.05
0
-0.05
0
2
4
6
8
10
Ambient Acceleration
(b)
×10^-3
3
2.5
2
1.5
1
0.5
0
-0.5
-1
-1.5
0
0.05
0.1
0.15
0.2
0.25

Figure

Click here to download Figure Figure 7.tif

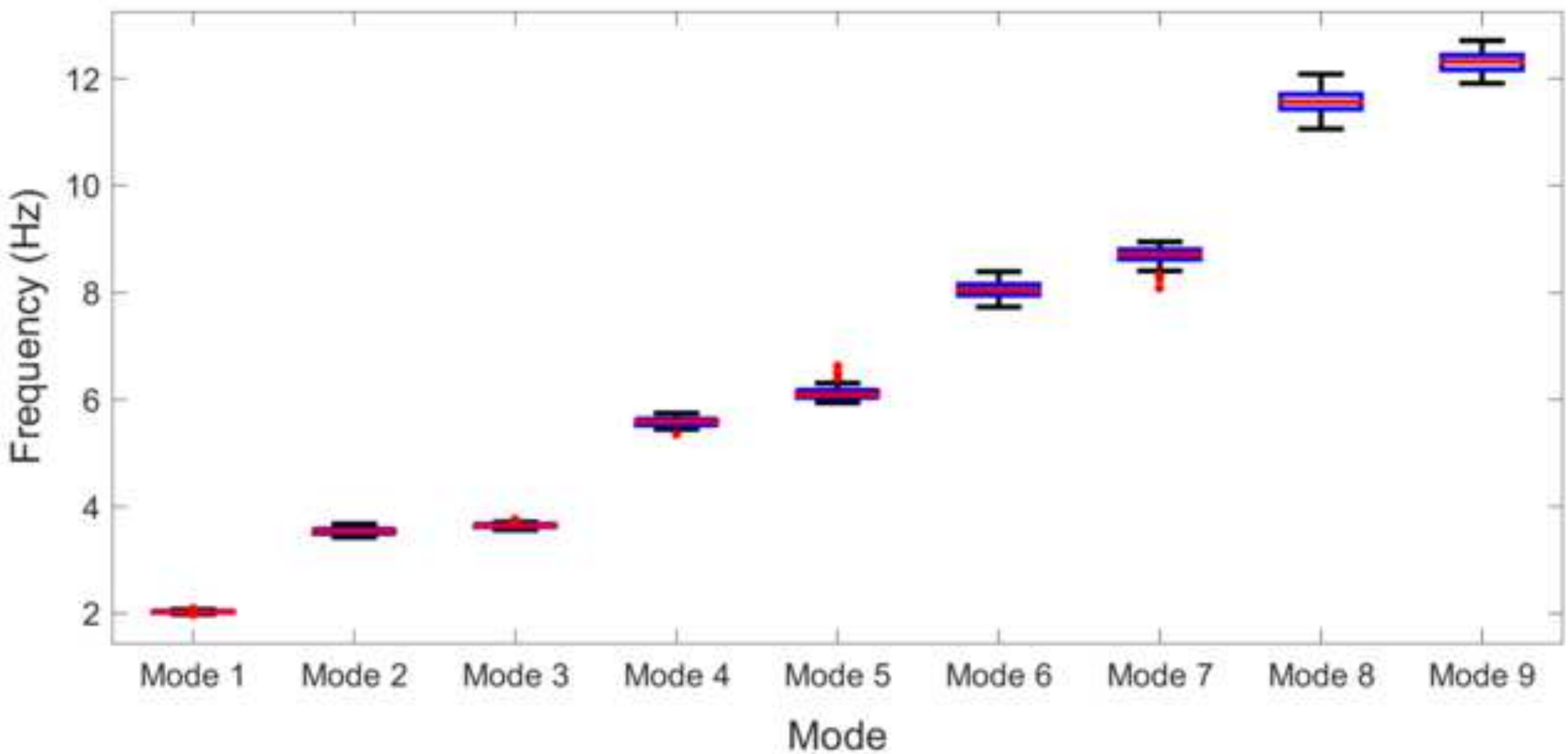

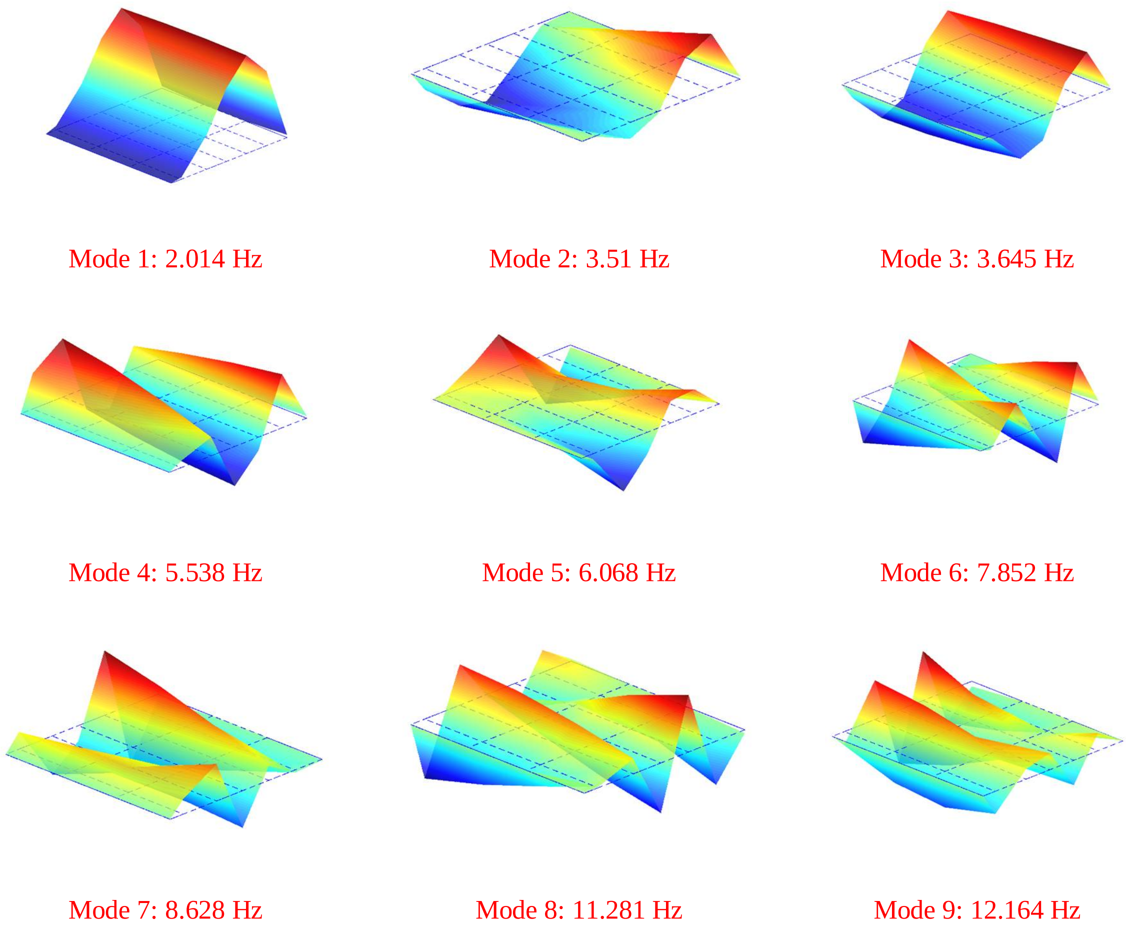
Mode 1: 2.014 Hz
Mode 2: 3.51 Hz
Mode 3: 3.645 Hz
Mode 4: 5.538 Hz
Mode 5: 6.068 Hz
Mode 6: 7.852 Hz
Mode 7: 8.628 Hz
Mode 8: 11.281 Hz
Mode 9: 12.164 Hz

Figure

Click here to download Figure Figure 9.tif

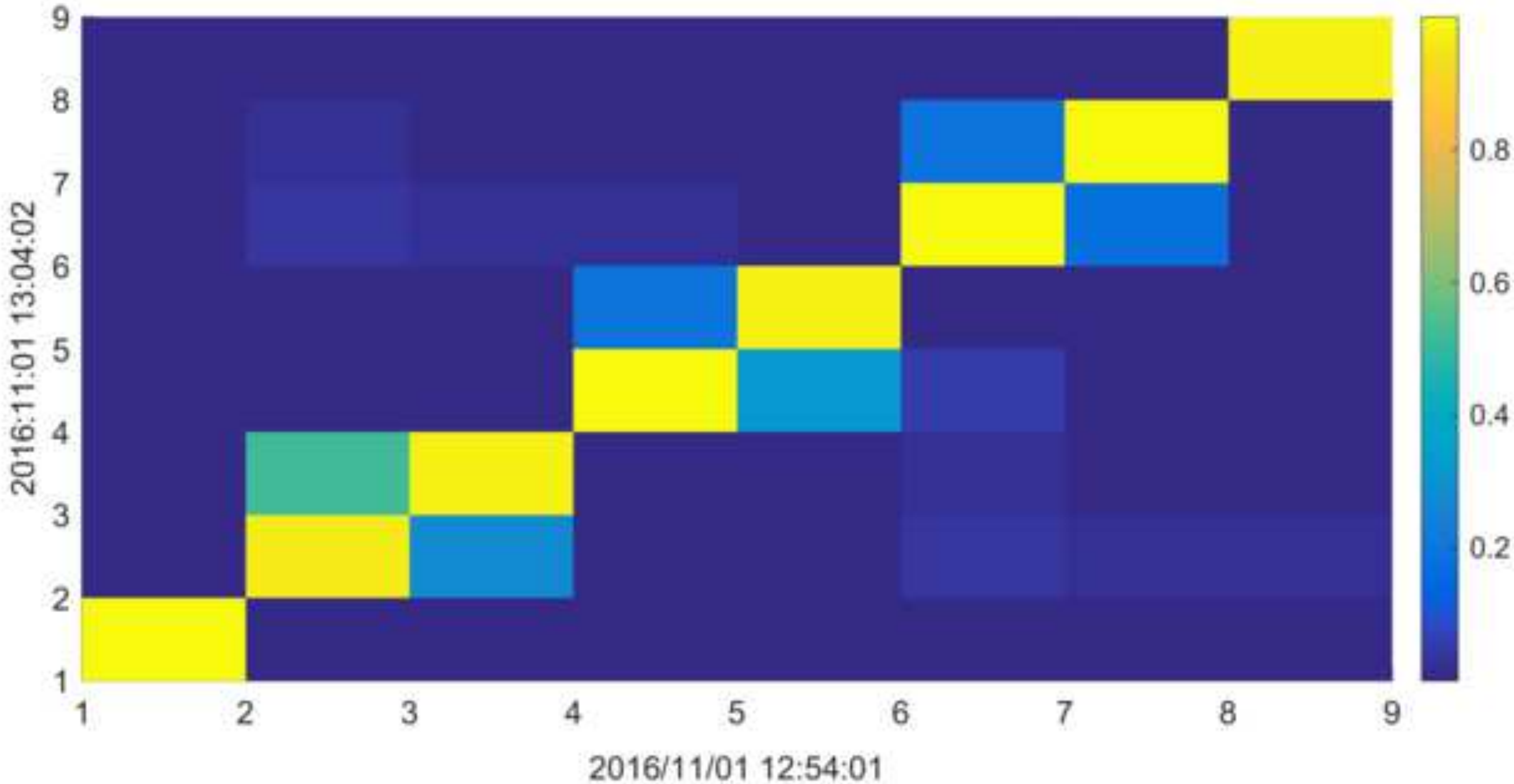

(a)

(b)

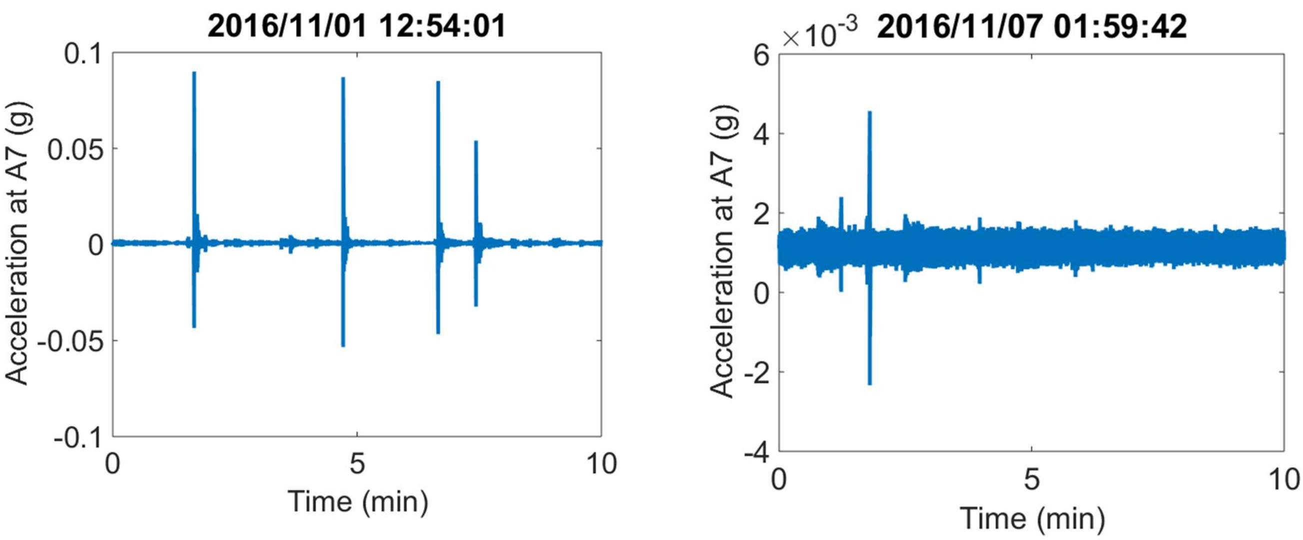
2016/11/01 12:54:01
0.1
0.05
0
-0.05
-0.1
Acceleration at A7 (g)
0
5
10
Time (min)
×10^-3
2016/11/07 01:59:42
6
4
2
0
-2
-4
Acceleration at A7 (g)
0
5
10
Time (min)

(a)

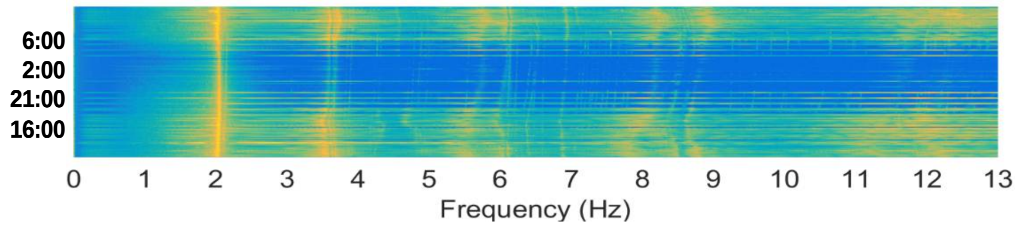
6:00
2:00
21:00
16:00
0 1 2 3 4 5 6 7 8 9 10 11 12 13
Frequency (Hz)

(b)

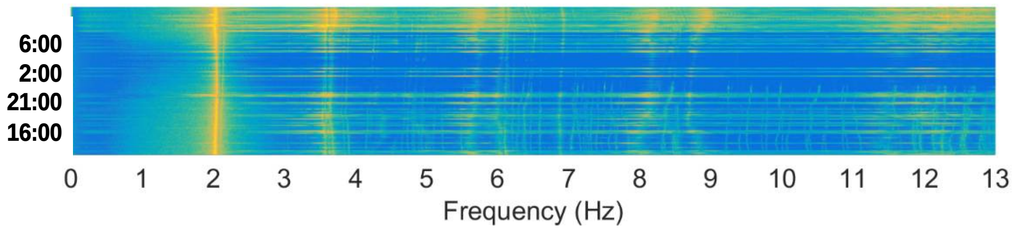
6:00
2:00
21:00
16:00
0 1 2 3 4 5 6 7 8 9 10 11 12 13
Frequency (Hz)

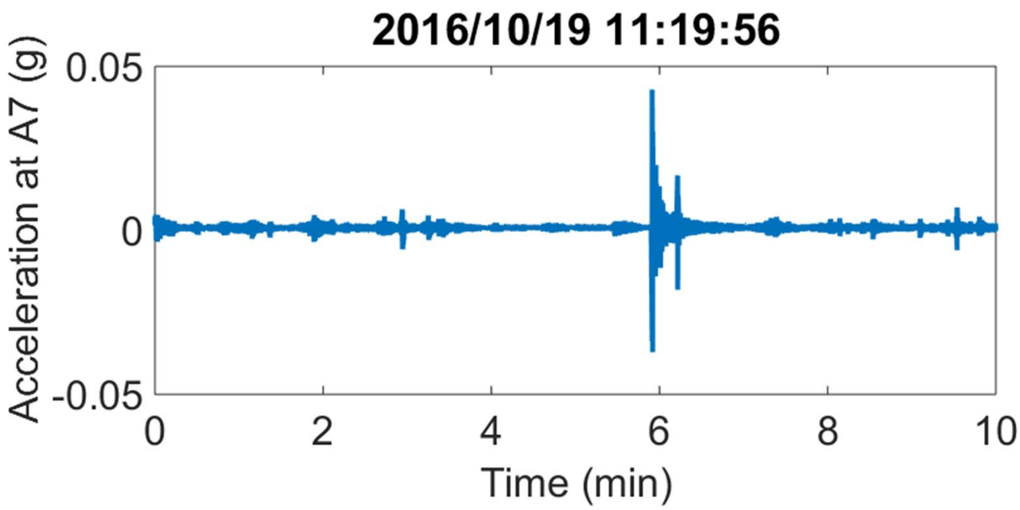
2016/10/19 11:19:56
Acceleration at A7 (g)
0.05
0
-0.05
0
2
4
6
8
10
Time (min)

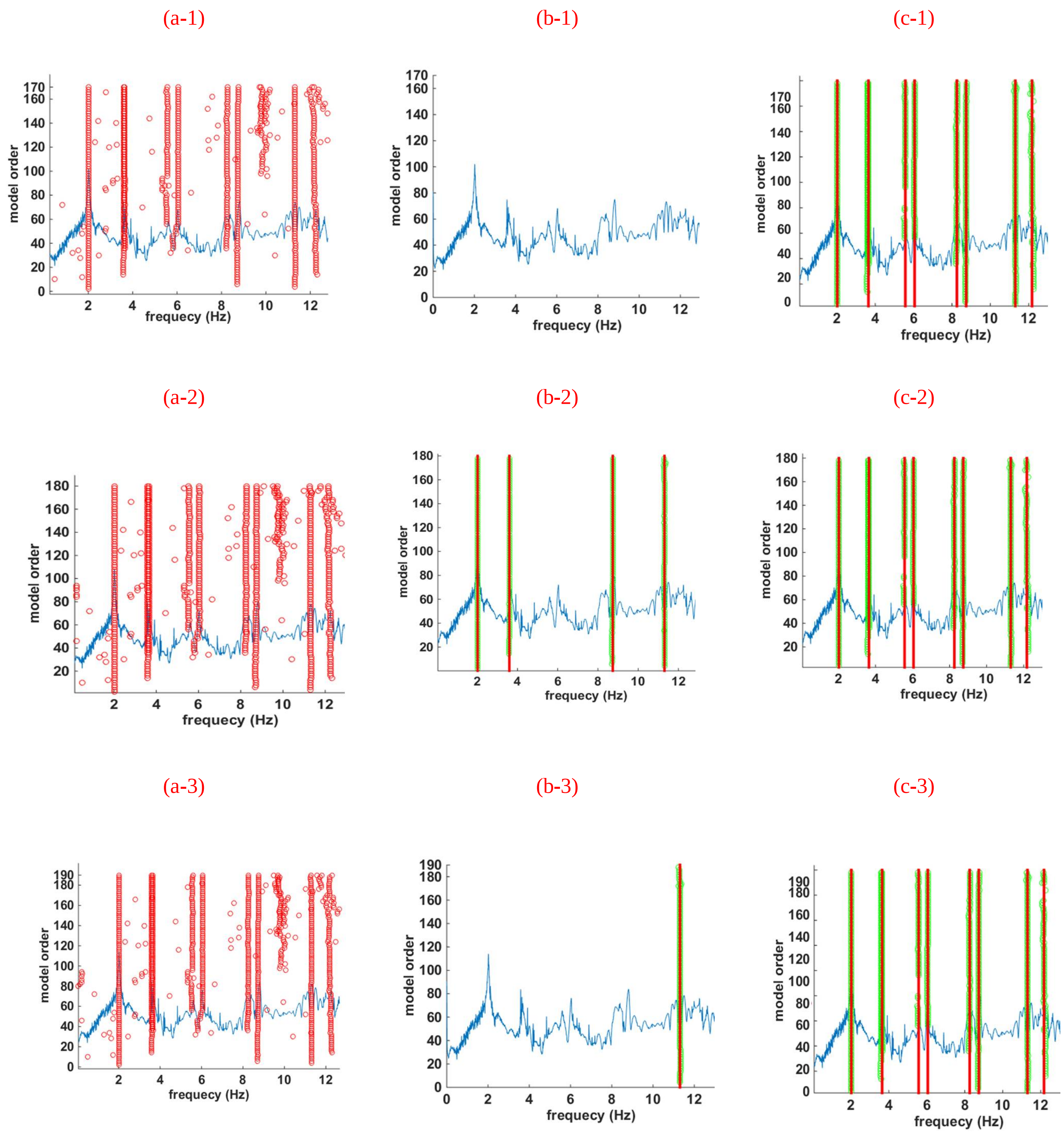
(a-1)
(b-1)
(c-1)
(a-2)
(b-2)
(c-2)
(a-3)
(b-3)
(c-3)
model order
frequecy (Hz)

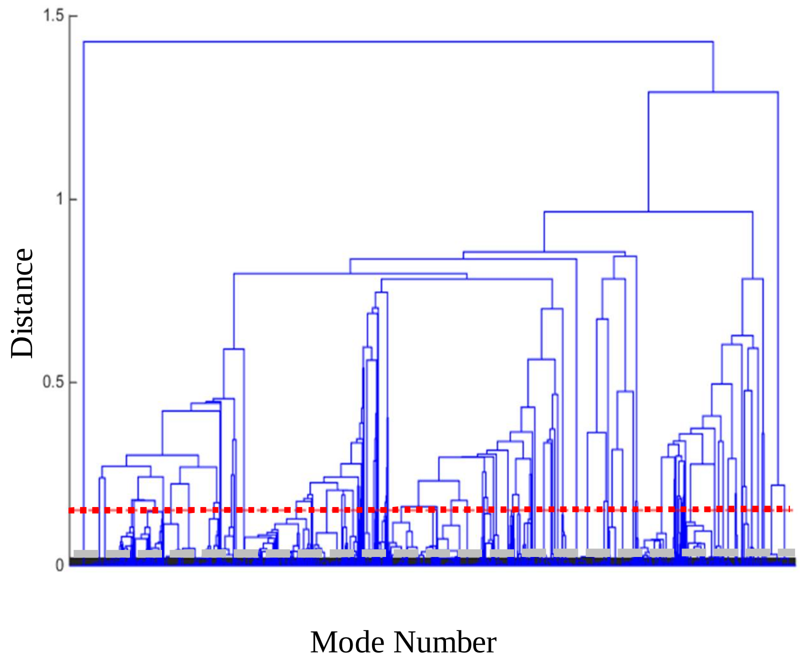
1.5
1
0.5
0
Distance
Mode Number

Figure

Click here to download Figure Figure 15.pdf

(a) (b)

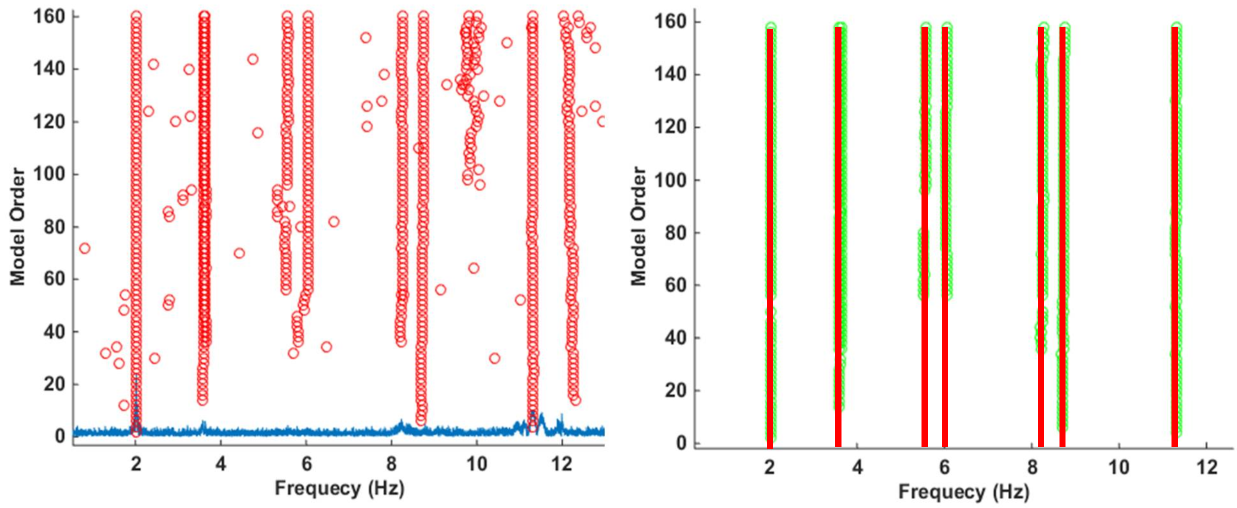

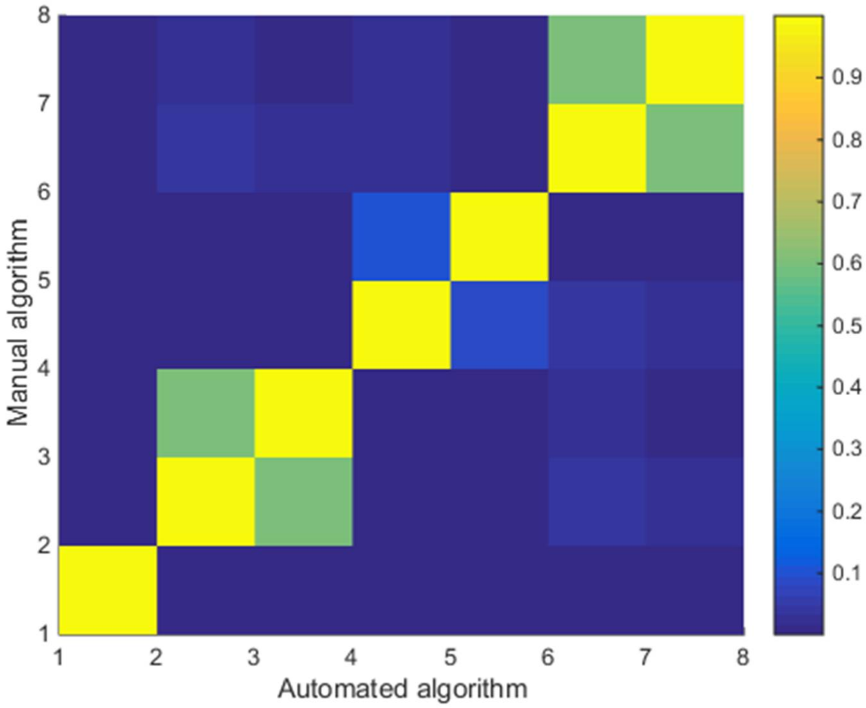
Manual algorithm
Automated algorithm
1
2
3
4
5
6
7
8
0.1
0.2
0.3
0.4
0.5
0.6
0.7
0.8
0.9

Figure 1. Illustration of SSI-Cov algorithm flowchart adopted in this work.

Figure 2. A cable stayed bridge over the Great Western Highway NSW Australia (Ref. Google Earth), (a) side view, (b) top view.

Figure 3. Illustration of deck, steel girders and floor beams.

Figure 4. The accelerometer array on the deck.

Figure 5. Illustration of the attached uni-axial accelerometer under the girder.

Figure 6. (a) Typical 10-minutes acceleration time history including response as a result of passing traffic, (b) typical ambient part of the response while there is no vehicle on the bridge.

Figure 7. The boxplot of the first nine modes extracted from 66 datasets.

Figure 8. Illustration of the first nine mode shapes of the deck.

Figure 9. Orthogonality check using MAC between the identified modes from two different datasets.

Figure 10. Illustration of acceleration response collected by sensor A7 while, (a) all of the nine modes have been extracted, (b) only the first mode has been identified.

Figure 11. Illustration of the spectrogram of acceleration response for (a) weekday, (b) weekend.

Figure 12. Illustration of a 10-minute acceleration response collected by sensor A7.

Figure 13. (a) Unfiltered stabilization diagram, (b) filtered stabilization diagram using the old threshold, (c) filtered stabilization diagram using the new threshold. (1) system order= 170, (2) system order = 180, (3) system order = 190.

Figure 14. Illustration of dendrogram of the hierarchical clustering (system order 170) and the cut-off distances using the old threshold (red dotted line) and the new threshold (grey dashed line).

Figure 15. (a) The unfiltered stabilization diagram and; (b) the filtered stabilization diagram obtained from the manual SSI-Cov algorithm.

Figure 16. Orthogonality check using MAC between the identified modes from the manual and automated algorithms.

ASCE Authorship, Originality, and Copyright Transfer Agreement

Publication Title: Journal of Bridge Engineering

Manuscript Title: Automated Operational Modal Analysis of a Cable-Stayed Bridge

Author(s) – **Names, postal addresses, and e-mail addresses of all authors**

Miao Sun, CSIRO, Data61, Eveleigh, Australia, smiaos@hotmail.com

Mehri Makki Alamdari, CSIRO, Data61, Eveleigh, Australia, Mehri.Makkialamdari@data61.csiro.au

Hamed Kalhori, CSIRO, Data61, Eveleigh, Australia, Hamed.Kalhori@data61.csiro.au

I. Authorship Responsibility

To protect the integrity of authorship, only people who have significantly contributed to the research or project and manuscript preparation shall be listed as coauthors. The corresponding author attests to the fact that anyone named as a coauthor has seen the final version of the manuscript and has agreed to its submission for publication. Deceased persons who meet the criteria for coauthorship shall be included, with a footnote reporting date of death. No fictitious name shall be given as an author or coauthor. An author who submits a manuscript for publication accepts responsibility for having properly included all, and only, qualified coauthors.

I, the corresponding author, confirm that the authors listed on the manuscript are aware of their authorship status and qualify to be authors on the manuscript according to the guidelines above.

Mehri Makki Alamdari		31/03/2017
Print Name	Signature	Date

II. Originality of Content

ASCE respects the copyright ownership of other publishers. ASCE requires authors to obtain permission from the copyright holder to reproduce any material that (1) they did not create themselves and/or (2) has been previously published, to include the authors' own work for which copyright was transferred to an entity other than ASCE. Each author has a responsibility to identify materials that require permission by including a citation in the figure or table caption or in extracted text. Materials re-used from an open access repository or in the public domain must still include a citation and URL, if applicable. At the time of submission, authors must provide verification that the copyright owner will permit re-use by a commercial publisher in print and electronic forms with worldwide distribution. For Conference Proceeding manuscripts submitted through the ASCE online submission system, authors are asked to verify that they have permission to re-use content where applicable. Written permissions are not required at submission but must be provided to ASCE if requested. Regardless of acceptance, no manuscript or part of a manuscript will be published by ASCE without proper verification of all necessary permissions to re-use. ASCE accepts no responsibility for verifying permissions provided by the author. Any breach of copyright will result in retraction of the published manuscript.

I, the corresponding author, confirm that all of the content, figures (drawings, charts, photographs, etc.), and tables in the submitted work are either original work created by the authors listed on the manuscript or work for which permission to re-use has been obtained from the creator. For any figures, tables, or text blocks exceeding 100 words from a journal article or 500 words from a book, written permission from the copyright holder has been obtained and supplied with the submission.

Mehri Makki Alamdari		31/03/2017
Print name	Signature	Date

III. Copyright Transfer

ASCE requires that authors or their agents assign copyright to ASCE for all original content published by ASCE. The author(s) warrant(s) that the above-cited manuscript is the original work of the author(s) and has never been published in its present form.

The undersigned, with the consent of all authors, hereby transfers, to the extent that there is copyright to be transferred, the exclusive copyright interest in the above-cited manuscript (subsequently called the "work") in this and all subsequent editions of the work (to include closures and errata), and in derivatives, translations, or ancillaries, in English and in foreign translations, in all formats and media of expression now known or later developed, including electronic, to the American Society of Civil Engineers subject to the following:

- The undersigned author and all coauthors retain the right to revise, adapt, prepare derivative works, present orally, or distribute the work, provided that all such use is for the personal noncommercial benefit of the author(s) and is consistent with any prior contractual agreement between the undersigned and/or coauthors and their employer(s).
- No proprietary right other than copyright is claimed by ASCE.
- If the manuscript is not accepted for publication by ASCE or is withdrawn by the author prior to publication (online or in print), or if the author opts for open-access publishing during production (journals only), this transfer will be null and void.
- Authors may post a PDF of the ASCE-published version of their work on their employers' ***Intranet*** with password protection. The following statement must appear with the work: "This material may be downloaded for personal use only. Any other use requires prior permission of the American Society of Civil Engineers."
- Authors may post the ***final draft*** of their work on open, unrestricted Internet sites or deposit it in an institutional repository when the draft contains a link to the published version at www.ascelibrary.org. "Final draft" means the version submitted to ASCE after peer review and prior to copyediting or other ASCE production activities; it does not include the copyedited version, the page proof, a PDF, or full-text HTML of the published version.

Exceptions to the Copyright Transfer policy exist in the following circumstances. Check the appropriate box below to indicate whether you are claiming an exception:

☐ **U.S. GOVERNMENT EMPLOYEES:** Work prepared by U.S. Government employees in their official capacities is not subject to copyright in the United States. Such authors must place their work in the public domain, meaning that it can be freely copied, republished, or redistributed. In order for the work to be placed in the public domain, ALL AUTHORS must be official U.S. Government employees. If at least one author is not a U.S. Government employee, copyright must be transferred to ASCE by that author.

☐ **CROWN GOVERNMENT COPYRIGHT:** Whereby a work is prepared by officers of the Crown Government in their official capacities, the Crown Government reserves its own copyright under national law. If ALL AUTHORS on the manuscript are Crown Government employees, copyright cannot be transferred to ASCE; however, ASCE is given the following nonexclusive rights: (1) to use, print, and/or publish in any language and any format, print and electronic, the above-mentioned work or any part thereof, provided that the name of the author and the Crown Government affiliation is clearly indicated; (2) to grant the same rights to others to print or publish the work; and (3) to collect royalty fees. ALL AUTHORS must be official Crown Government employees in order to claim this exemption in its entirety. If at least one author is not a Crown Government employee, copyright must be transferred to ASCE by that author.

☐ **WORK-FOR-HIRE:** Privately employed authors who have prepared works in their official capacity as employees must also transfer copyright to ASCE; however, their employer retains the rights to revise, adapt, prepare derivative works, publish, reprint, reproduce, and distribute the work provided that such use is for the promotion of its business enterprise and does not imply the endorsement of ASCE. In this instance, an authorized agent from the authors' employer must sign the form below.

☐ **U.S. GOVERNMENT CONTRACTORS:** Work prepared by authors under a contract for the U.S. Government (e.g., U.S. Government labs) may or may not be subject to copyright transfer. Authors must refer to their contractor agreement. For works that qualify as U.S. Government works by a contractor, ASCE acknowledges that the U.S. Government retains a nonexclusive, paid-up, irrevocable, worldwide license to publish or reproduce this work for U.S. Government purposes only. This policy DOES NOT apply to work created with U.S. Government grants.

I, the corresponding author, acting with consent of all authors listed on the manuscript, hereby transfer copyright or claim exemption to transfer copyright of the work as indicated above to the American Society of Civil Engineers.

Mehri Makki Alamdari

Print Name of Author or Agent

31/03/2017

Signature of Author of Agent — Date

More information regarding the policies of ASCE can be found at http://www.asce.org/authorsandeditors

Journal of Bridge Engineering

Automated Operational Modal Analysis of a Cable-Stayed Bridge

Miao Sun, Mehrisadat Makki Alamdari*, Hamed Kalhori

*Corresponding author: Mehri.Makkialamdari@data61.csiro.au

CSIRO, Data61, 13 Garden Street, Eveleigh NSW 2015, AUSTRALIA

First of all, we apologize for the low quality of the first draft of the paper, mainly caused by the lack of available data, which prevented us from conducting a comprehensive investigation. We appreciate the constructive feedback from the reviewers. This report provides detailed answers to all of the comments suggested by the reviewers. Accordingly, significant modifications were made in the manuscript in order to address these points. All the changes were made with red color in the revised paper.

Since some of the comments raised by the reviewers were in common, to avoid unnecessary duplications, we have referred to the answers provided earlier in the report for those questions which are repetitive; therefore, it is the authors request to share the entire document with all three reviewers.

Please find our responses to the comments as detailed below.

1. Reviewer I

"This paper aims to present an automated operational modal analysis algorithm without the need of user interactions. The proposed algorithm is applied to the identification of a cable-stayed bridge structure through several case studies using real data. The paper is interesting but more clarifications and revisions are needed before it can be accepted."

1.1 Reviewer 1 - Comment 1

"As indicated in the introduction part of this paper, the proposed algorithm is developed based on the ideas of clustering approaches for automated OMA by Reynders et al. (reference 16). In Sect. 3 on automated algorithm for stabilization process, all the modal validation criteria are the same as those in references 16 and 18. Also, the reviewer is aware of many similar algorithms have been developed for automated operational modal analyses. Therefore, the technical innovations of the proposed algorithm should be compared with previous ones in details."

Response:

As mentioned in the first draft of the paper, the main contribution of the work is to define a novel way of automatically defining the hierarchical clustering threshold, d_H to enable the accurate identification of a complete set of modal parameters, regardless of the system order chosen. Previous works suggested a d_H value based on the mean and standard deviations of the probably physical mode distances as (Reynders et al. 2012; Rubén and Joaquín 2015):

$$d_H = \mu_{C_R} + 2\sigma_{C_R}$$

where the μ_{C_R} and σ_{C_R} are the sample mean and sample standard deviation, respectively, of the mutual distance values.

In this study, a novel approach to identify d_H, was proposed which provides reliable modal identification results, regardless of the system order selected. At each model order m, the mutual distance between every two poles is calculated and the minimum distance is determined. The threshold value d_H is selected as the median value of the minimum distances obtained for all the model orders. The median value is capable of more effectively eliminating the impact of outliers. In the first draft of the paper, the discussion on superiority of this newly established threshold (new threshold) over the previous one proposed by Reynders (old threshold) was limited; however, significant improvement was carried out to resolve this problem.

For a typical 10-minute acceleration response collected from the bridge, shown in Figure 1 (for all the details/ changes made in the measurement set-up and data collection procedure, please see Section 4 of the revised paper), the SSI-Cov technique was applied (the parameters and details have been elaborated in Section 4 of the revised paper). Five different system orders ranging from 160 to 200 with an increment of 10 were considered. Both the new and the old thresholds were adopted and the results were compared. Table 1 and Table 2, respectively, summarize the identified modes using the old and the new thresholds. As seen, the old threshold can only provide successful identification of the modes where the system order is 160 and it fails to identify the modes for the other system orders, i.e. 170, 180, 190 and 200. However, by using the new threshold all the modes are successfully identified no matter what system order is considered.

Figure 2 illustrates the stabilization diagrams for the system orders 170, 180 and 190. Column (a) is the unfiltered stabilization diagram, column (b) is the filtered stabilization diagram using the old threshold and column (c) is the filtered stabilization diagram using the new threshold. Consistent to the results presented in Table 1 and Table 2, it is clear that the old threshold fails to identify the modes even at situations that they look stable. In contrast, by utilizing the new threshold, all the modes even the closely-spaced mods are successfully identified. Please note that in the filtered stabilization diagram using the new threshold there are two closely-spaced modes around 3.5 Hz (3.597 Hz and 3.643 Hz). System order 200 provides similar result to the one obtained from the system order 190 and because of space restrictions it was not presented. This investigation implies that the procedure of eliminating the spurious modes using the new threshold is effective and as a result, the homogeneous groups of modes which represent the real physical modes are clearly detected.

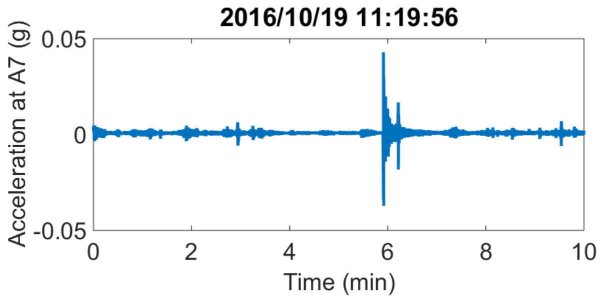

Figure 1. Illustration of a 10-minute acceleration response collected by sensor A7.

Table 1. Identification results using the old threshold.

System Order	ω_1	ω_2	ω_3	ω_4	ω_5	ω_6	ω_7	ω_8	ω_9
160	2.017	3.570	3.643	5.569	6.046	8.257	8.739	11.309	12.172
170	---	---	---	---	---	---	---	---	---
180	2.017	3.597	---	---	---	---	8.739	11.309	---
190	---	---	---	---	---	---	---	11.305	---
200	---	---	---	---	---	---	---	11.305	---

Table 2. Identification results using the new threshold.

System Order	ω_1	ω_2	ω_3	ω_4	ω_5	ω_6	ω_7	ω_8	ω_9
160	2.017	3.597	3.643	5.568	6.044	8.255	8.739	11.309	12.176
170	2.017	3.597	3.643	5.568	6.051	8.255	8.740	11.309	12.176
180	2.017	3.597	3.643	5.568	6.051	8.255	8.740	11.307	12.176
190	2.017	3.597	3.643	5.568	6.051	8.255	8.739	11.307	12.176
200	2.017	3.597	3.643	5.568	6.051	8.255	8.740	11.305	12.177

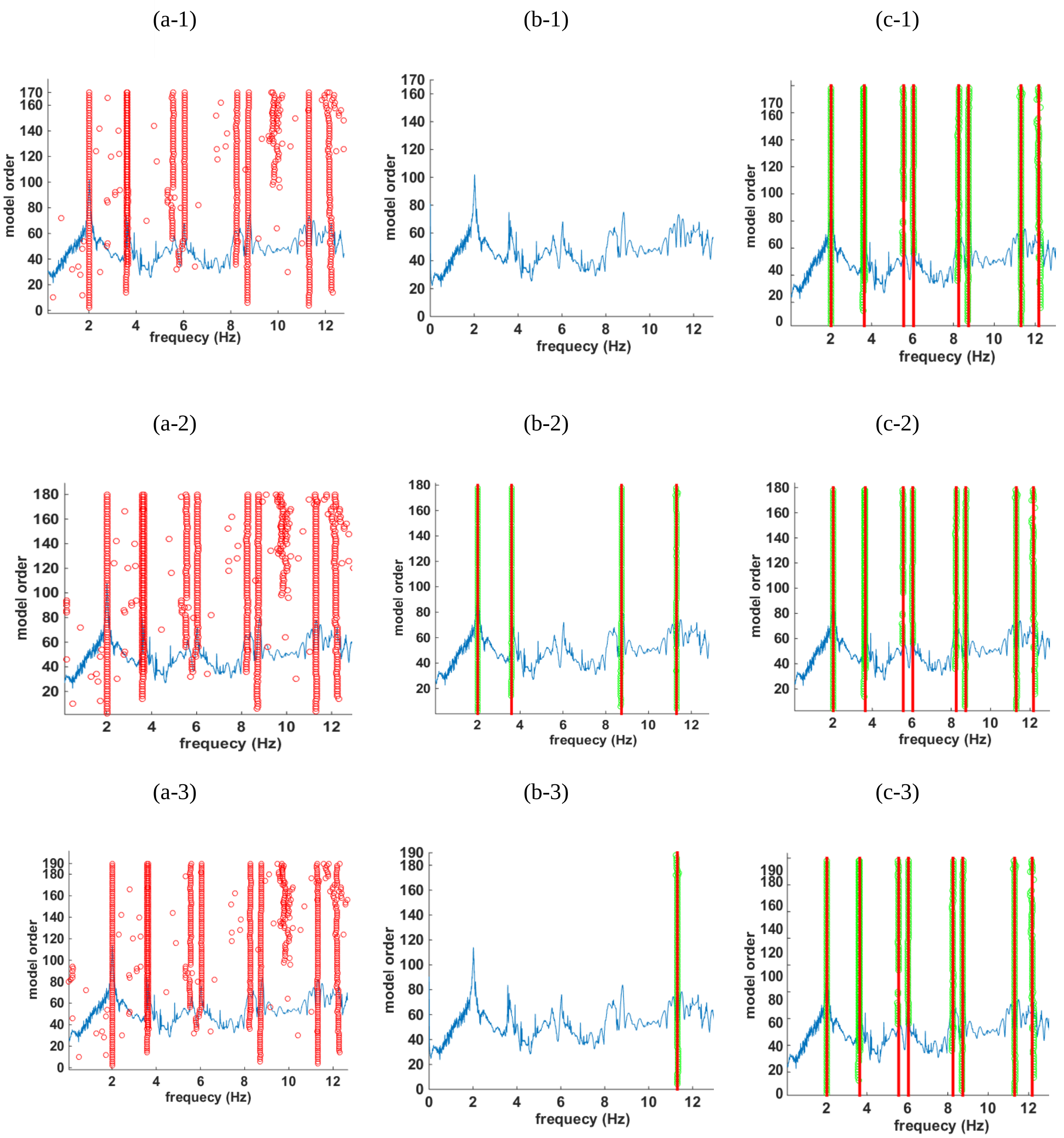

Figure 2. (a) unfiltered stabilization diagram, (b) filtered stabilization diagram using the old threshold, (c) filtered stabilization diagram using the new threshold. (1) system order= 170, (2) system order = 180, (3) system order = 190.

To further investigate the superiority of the new threshold over the old threshold, the dendrogram of the hierarchical clustering for the system order 170 was studied and the result was shown in Figure 3. The red dotted line and the grey dashed line, respectively, illustrate the position of the cut-off distances for the hierarchical clustering obtained by the old and the new thresholds. It is clear that the new threshold proposes a much lower threshold (0.0040) than the old threshold (0.1513) for system order 170. As indicated by the identification results, within the frequency range of 0-13Hz, nine structural modes have been successfully identified with the new threshold however no structural mode is identified using the old threshold. These results imply that the old threshold value is too high for the hierarchical clustering. In hierarchical clustering, modes with similar attributes are linked to each other to produce the dendrogram. Ideally, the threshold value signifies that each tree underneath the threshold should represent a single real structural mode. However, because the old threshold is much higher than the desired threshold, distinct modes have been merged into the same cluster. This usually results in one big cluster containing many modes of distinctive frequencies, where the total number of the modes in this cluster is much greater than the number of the modes in the other clusters. Consequently, during the next stage of the algorithm, where the second *k*-means clustering is applied, based on the number of the modes in each cluster, the largest cluster significantly overweighs the other smaller clusters and thus the smaller clusters are classified as the clusters with spurious modes.

The authors hope that the above explanation is adequate enough to answer the reviewer's comment, however, we are more than happy to provide further details if required.

Revised text:

Please look at Section 5 in the revised paper.

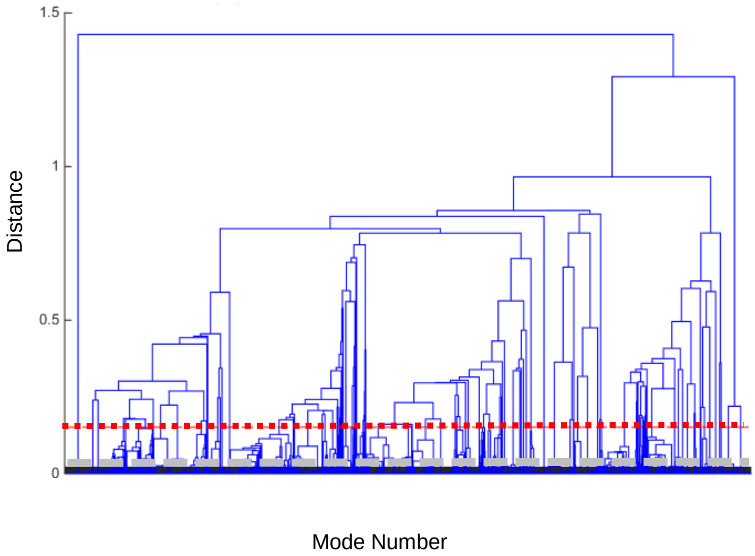

Figure 3. Illustration of dendrogram of the hierarchical clustering (system order 170) and the cut-off distances using the old threshold (red dotted line) and the new threshold (grey dashed line).

1.2 Reviewer 1 - Comment 2

"Although it is claimed that a novel approach for the hierarchical clustering process is proposed, it is essential to compare the numerical identification results by the proposed approach with those by previous ones."

Response:

Please look at the response provided to Reviewer 1 – Comment 1.

1.3 Reviewer 1 - Comment 3

"In Table 2, some modal parameters extracted by the proposed automated approaches are missed by the manual analyses. The reviewer wanders this superiority of the automated approaches."

Response:

The manual cleaning of the stabilization diagram is performed based on the pre-defined frequency tolerance (t_f), damping ratio tolerance (t_ξ), and MAC value. Obviously, the smaller values of t_f and t_ξ and a larger value of MAC indicate more strict tolerances, resulting in identification of the most dominant modes of the structures. These modes are actually the ones that consistently appear in the stabilization diagram as stable modes. Hence, for the strict tolerances, we are confident that most of the identified modes are real, however, we may potentially miss some real modes because they do not satisfy the defined tolerances.

The results presented in Table 2 of the first version of the paper were basically obtained from random values of t_f, t_ξ and MAC. To investigate the effect of the parameters to be manually tuned for cleaning of the stabilization diagram, sufficiently excited datasets were chosen. Table 3 compares the first nine natural frequencies of the bridge obtained from the manual algorithm for different values of t_f, t_ξ and

MAC values with the modes obtained from the automated algorithm. For very strict tolerances ($t_f = 0.001, t_\xi = 0.005$ and MAC=0.99), a few number of modes are identified. However, less strict tolerances result in identification of a larger number of modes, as expected. The tolerance set of t_f, t_ξ and MAC, respectively, equal to 0.010, 0.100, and 0.99 looks suitable as the damping ratio tolerance is neither very small nor very large. This tolerance set leads to identification of the first eight modes. Figures 4 (a) and (b), respectively, show the original (unfiltered) stabilization diagram and the filtered stabilization diagram obtained from the manual SSI-Cov algorithm using this tolerance set. By making the tolerances less strict, additional modes are identified, where the majority of them vary between 20 Hz and 50 Hz. However, chances are high that some of these additional modes are spurious. It should also be noticed that none of the tolerance sets in Table 3 resulted in identifying the ninth mode, whereas, this mode is identified by the automated algorithm and is visually identifiable in the unfiltered stabilization diagram as depicted in Figure 4 (a).

As a general conclusion, finding the most appropriate tolerance values is the key factor in the manual algorithm so that as many real modes as possible are identified and, at the same time, no spurious modes are generated. This highlights the importance of the automated parameter tuning and also the superiority of the automatic algorithm.

Table 3. Natural frequencies obtained from the automated SSI-Cov algorithm and the manual SSI-Cov algorithm for different values of frequency tolerance (t_f), damping ratio tolerance (t_ξ), and MAC.

Manual algorithm

Manual parameters t_ξ, t_f, MAC	ω_1	ω_2	ω_3	ω_4	ω_5	ω_6	ω_7	ω_8	ω_9
0.005, 0.001, 0.99	2.017	3.597	3.643	---	---	---	8.740	---	---
0.008, 0.002, 0.99	2.017	3.597	3.643	---	---	8.255	8.739	---	---
0.010, 0.007, 0.99	2.017	3.597	3.643	---	6.044	8.262	8.747	---	---
0.050, 0.010, 0.99	2.017	3.596	3.644	---	6.044	8.262	8.740	11.303	---
0.100, 0.001, 0.99	2.017	3.596	3.644	---	6.044	8.255	8.747	11.304	---
0.100, 0.010, 0.99	2.017	3.596	3.643	5.568	6.044	8.258	8.747	11.293	---
0.100, 0.010, 0.95	2.017	3.596	3.643	5.568	6.044	8.258	8.747	11.293	---
0.100, 0.500, 0.95	2.017	3.596	3.643	5.568	6.044	8.258	8.747	11.293	---
0.500, 0.010, 0.95	2.017	3.596	3.643	5.579	6.044	8.258	8.747	11.293	---
0.800, 0.500, 0.95	2.017	3.596	3.643	5.561	6.044	8.258	8.747	11.291	---

Automated algorithm

ω_1	ω_2	ω_3	ω_4	ω_5	ω_6	ω_7	ω_8	ω_9
2.017	3.597	3.643	5.568	6.044	8.255	8.739	11.309	12.176

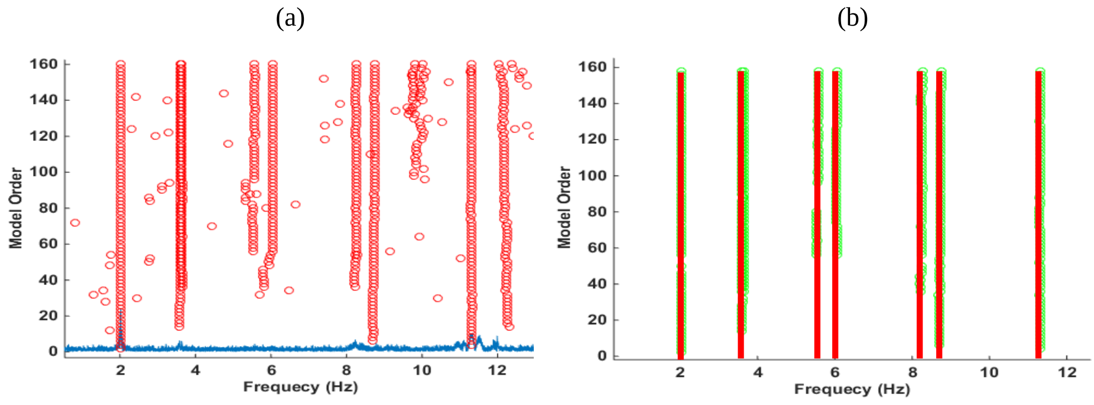

Figure 4. (a) The original (unfiltered) stabilization diagram and; (b) the filtered stabilization diagram obtained from the manual SSI-Cov algorithm.

1.4 Reviewer 1 - Comment 4

"From the results in Table 3, it is quite puzzled to explain the effect of vehicle passing velocity on the identification results as some modes may not be extracted with the increase of velocity."

Response:

First of all, the authors would like to emphasize that section "*5.2. Ambient vibration data at 600Hz with vehicle passing*" presented in the first draft of the paper has been eliminated since we believe there was not adequate amount of data from controlled vehicles passing over the bridge with various known speeds to enable us to perform a comprehensive investigation to fully understand the impact of vehicle speed on modal identification results. However, in order to investigate the effect of the ambient excitation on the modal identification results, further analyses were performed as outlined below.

In the revised version of the paper, significant effort has been made to study the long term vibrational behavior of the structure using the proposed technique of operational modal analysis; details of the experiments and results can be found in Sections 4 and 5 of the revised paper.

Basically, 22 days of monitoring data, continuously acquired from the 1st of November until the 22nd of November 2016 are used in the revised version of the paper for the purpose of the operational modal analysis. This selection was only made due to the availability of the data in this time period. For each day, three files were considered. The files were selected from different times within 24 hours including midnight, and rush traffic hours. This provides a total number of 66 10-minute-files for our investigations. The operational modal analysis adopting SSI-Cov algorithm was only performed on these 66 datasets (please note that in the revised version of the paper NExT-ERA has been eliminated, please look at the response provided to Reviewer 3 - Comment 2). Details on pre-processing of the data and the parameters adopted for the algorithm can be found in Section 4 of the revised paper.

Table 4 summarizes the identification results within the frequency range of [0-13 Hz]. As seen, within this frequency range, nine modes have been extracted including two closely-spaced modes around 3.5 Hz. It was realized that not all of the modes are extracted from every single dataset. The last column of Table 4 specifies the percentage of identification for each particular mode amongst 66 datasets. As shown, the first mode has been identified from all of the 66 datasets, however, the ninth mode have been identified only from 76% of datasets i.e. 50 datasets. A detailed discussion explaining the missed identification of some modes can be found in the next section.

ω_{mean} shows the mean value of the natural frequency for each mode obtained from 66 datasets and ω_{RSD} shows the relative standard deviation (RSD) for the identified natural frequencies; RSD is a standardized measure obtained by normalizing the standard deviation with respect to the mean value and it shows the dispersion of a distribution. A relative standard deviation of 1% to 2% is observed for the identified eigen-frequencies which is quite low and indicates the consistency of the modal identification over time. ξ_{mean} and ξ_{RSD}, respectively, show the mean damping ratio for each mode and the corresponding relative standard deviation. As illustrated in Table 4, the uncertainty on the damping ratio estimates is much higher than the uncertainty obtained for the natural frequencies and greater discrepancies are observed in damping estimation. Past research works (Magalhaes et al. 2009; Geothals et al. 2004) have also had similar observations and the explanation for this is that large scattering and dispersion are common for the damping ratios estimated from OMA methods. Rainieri et al. (2010) suggested that the presence of inherent limitations or inaccuracies of data processing methodologies can both lead towards high variations in damping ratio estimates. Inappropriate selection of the model order for the stabilization diagram may also enlarge the scattering of damping ratio for each identified mode. The high uncertainty in the identification of damping in civil structures can also be attributed to the fact that damping is strongly influenced by the magnitude of the dynamic response of a structure (Reynders et al. 2008).

Figure 5 illustrates the boxplot of the nine identified modes. Based on this figure, higher modes are experiencing higher standard deviation compared to the lower modes. Figure 6 shows the first nine mode shapes of the structure. Mode shape estimates were constructed using only the data locations corresponded to the measuring points in the testing and also zero deflection boundaries at supports. In the plan view presentation of each mode shape, an interpolating function is applied to provide a shaded approximation of the continuous mode shape. As seen in Figure 6, the reconstructed mode shapes encompass bending and torsional modes of the deck. Mode 1 is the first vertical bending mode of the deck which was consistently identified from all 66 datasets. Modes 2 and 3 make up a double mode which corresponds to the second vertical bending mode. Mode 4 corresponds to the third bending mode and modes 5 and 6 show a mixture of torsion and bending. The last three modes is a combination of the fourth bending mode and torsion.

Table 4. Modal identification results from 22 days of monitoring in November 2016.

Mode number	ω_{mean}	ω_{RSD} (%)	ξ_{mean} (%)	ξ_{RSD} (%)	Identified modes
1	2.032	0.98	0.9	42.23	100%
2	3.548	1.66	2.5	60.00	85%
3	3.649	1.15	2.2	63.14	81%
4	5.584	1.45	1.9	57.89	67%
5	6.136	2.33	2.8	42.85	82%
6	8.044	1.71	1.7	52.94	73%
7	8.671	2.09	1.7	70.58	60%
8	11.561	1.89	1.8	27.77	64%
9	12.31	1.46	1.4	42.86	76%

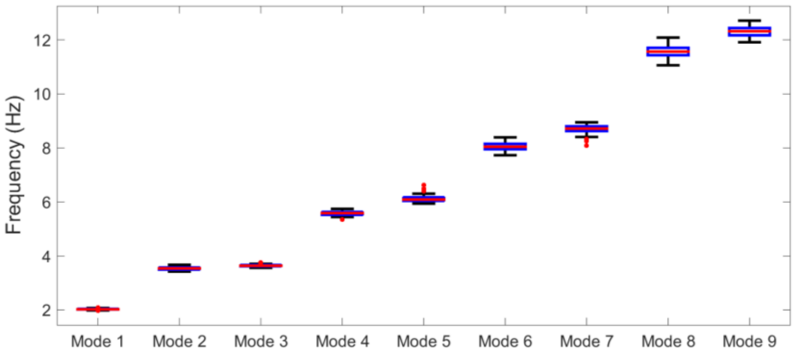

Figure 5. The boxplot of the first nine modes extracted from 66 datasets.

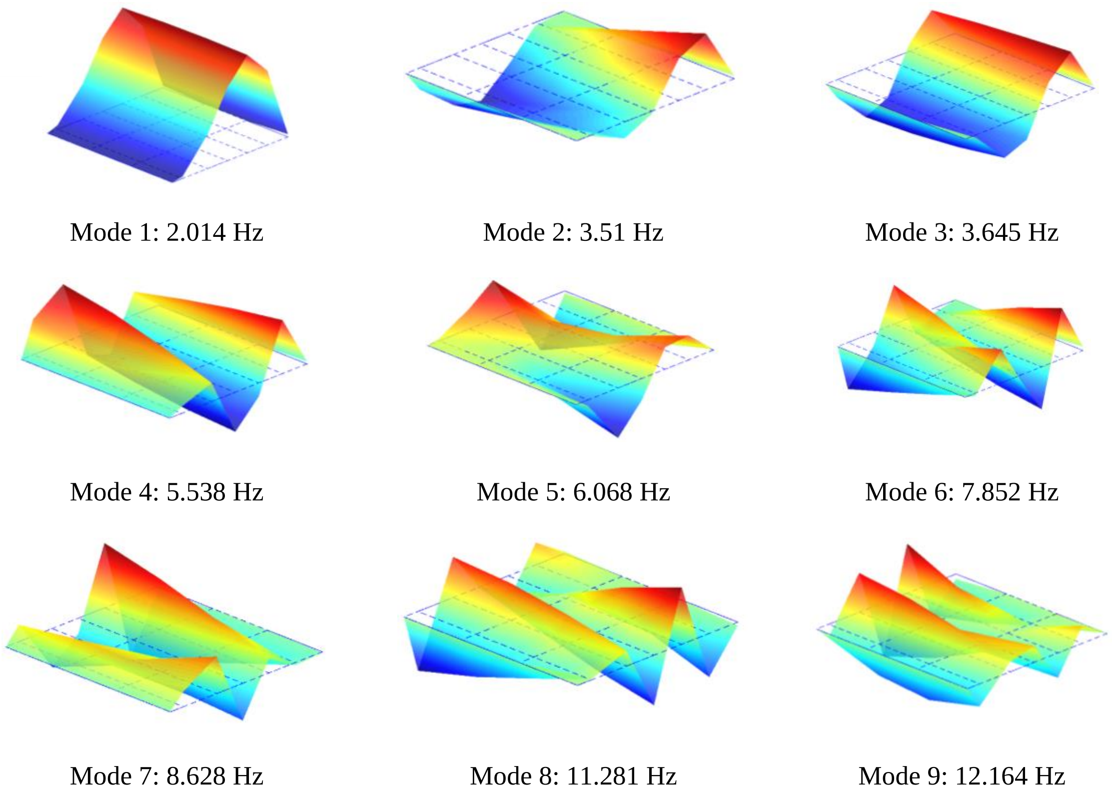

Figure 6. Illustration of the first nine mode shapes of the deck.

Consistency of Mode Shapes over Time

For any modal identification process, it is quite important to ensure the consistency of the mode shapes over time. MAC can be used for this purpose to quantify the correlation between the modes measured during different tests. MAC makes use of the orthogonality properties of the mode shapes to compare modes from different tests. If the modes are identical, a scalar value of one is calculated, otherwise it would be very small close to 0. The utilization of MAC can help for mode pairing to track a particular mode from different datasets and to see the consistency of identification of a particular mode between different datasets. For two arbitrary datasets, the MAC matrix was generated and it was illustrated in Figure 7. Basically, the horizontal axis shows the nine modes identified from a particular dataset and the vertical axis shows the identification results from a separate dataset. As seen, the diagonal MAC values are very high (>0.9) which shows the fact that the identified nine modes from two datasets are very similar and highly correlated. In general, very small MAC numbers are observed for off-diagonal members which is expected due to the orthogonality of the mode shapes. However, the closely-spaced modes 2 and 3 show some coupling through the off-diagonal MAC values. These results generally outline a very good agreement between the identified modes from different datasets. Similar graphs were obtained from different datasets and because of space restriction only one graph was presented.

The authors would like to emphasize that the procedure for calculation of the MAC values in the first draft of the paper (please see Figure 7 in the first draft) has not been correctly addressed. The reason is that the MAC had been calculated using the modes identified from a single dataset only and it is evident that all the diagonal members have to be 1 which does not add any value. This problem has been resolved in the revised version as elaborated above.

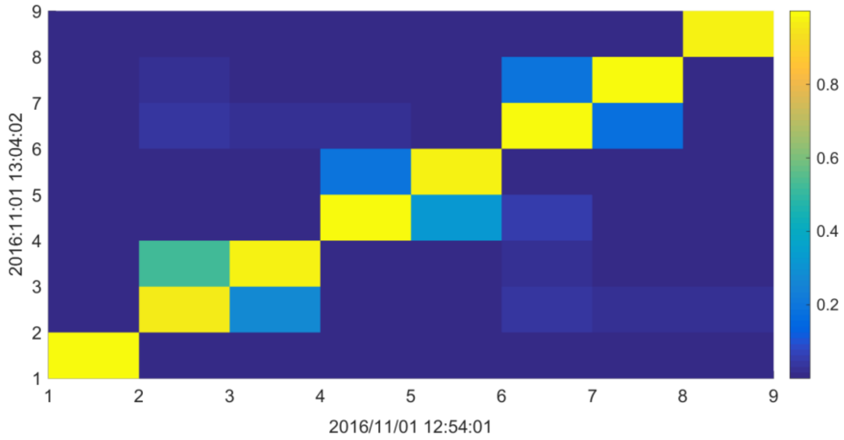

Figure 7. Orthogonality check using MAC between the identified modes from two different datasets.

Missed Identification

As discussed earlier, not all of the modes can be extracted from all 66 datasets. To further investigate the missed identification of some modes, the acceleration responses of the bridge (10 minutes) for two different cases were compared with each other: a case where only one mode, which is the first mode, has been identified, and a case that all of the nine modes have been identified. Figure 8 (a) illustrates the acceleration response obtained from channel 7 for a case that all modes have been extracted whereas

Figure 8 (b) shows the response for a case that only the first mode has been identified. From this figure, it is quite obvious that the level of response is almost 25 times higher in Figure 8 (a) compared to the response presented in Figure 8 (b) which coincides with the time windows of these two files, i.e. mid-day versus mid-night. It demonstrates the fact that if the ambient excitation on the bridge is not adequate enough, there is a high chance that the modes, in particular the higher modes, are not excited. To fully address the issue of missing modes, a separate study was conducted. This time, the vibration response of the bridge was collected from two different days: a working day and a weekend. Each day provides 24 hr×6 files/hr=144 10-minute files. Please note that the previously elaborated datasets including 66 files from 22 days of monitoring in November 2016 are the main datasets which have been adopted for our investigations in this paper and the continuous 24 hour data from these two days i.e. one weekday and one weekend has been solely adopted to further validate the impact of ambient excitation on missing modes and no further data analysis has been done using these datasets.

For each file, (in total, 144 files per day) the first singular value of SVD (Singular Value Decomposition) of spectral density matrix was calculated. This provides an estimation of the auto spectral density of the system in modal coordinates and the peak in the SVD curve is expected to represent a structural mode. Figure 9 (a) and (b), respectively, show the spectrograms of the response combining all of the 144 files from 24 hours for a weekday and for a weekend. The horizontal axis in these figures is frequency and the vertical axis is the time within 24 hours. The starting time in the vertical axis is almost 11:00 am. The color reflects the strength of the frequency component, i.e. the lighter the shade is, the higher the strength of the frequency component is. From this figure, it is quite evident that the first mode has been well excited at any time within the 24 hours during weekday and weekend. This figure also implies that modal identification process fails to extract the modes while there is not enough traffic on the bridge i.e. the time window between 8:00 pm to 6:00 am. It can also be observed that within the time window of 6:00 am to 8:00 pm the identification process has been more successful on weekday rather than weekend, again due to sufficiency of excitation on the bridge as a result of passing traffic. Additional piece of information that can be captured from this figure is that there is frequency variation in the modal frequencies which can be related to the environmental changes within 24 hours. From these investigations it appears that while the excitation level during ambient vibration is insufficient to produce reasonably strong vibration, the estimation process more likely fails to extract all of the modes particularly the higher modes.

(a) (b)

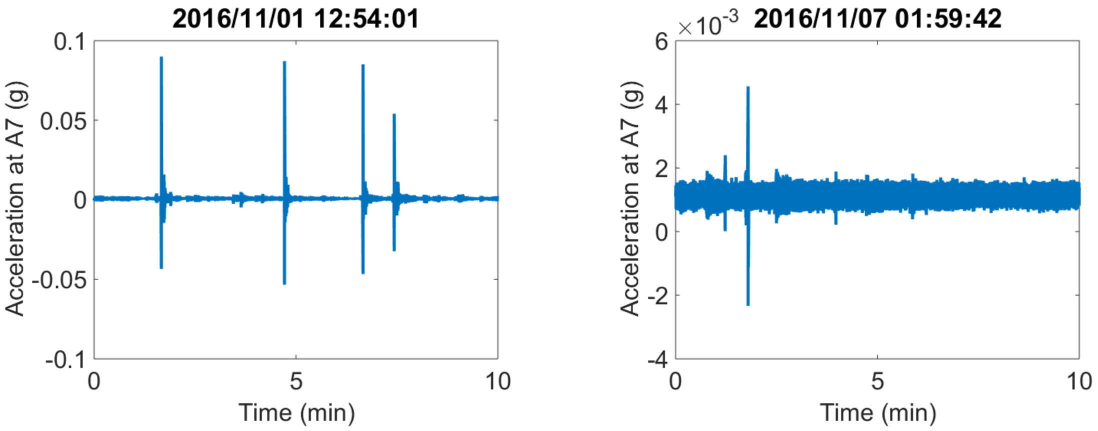

Figure 8. Illustration of acceleration response collected by sensor A7 while, (a) all of the nine modes have been extracted, (b) only the first mode has been identified.

(a)

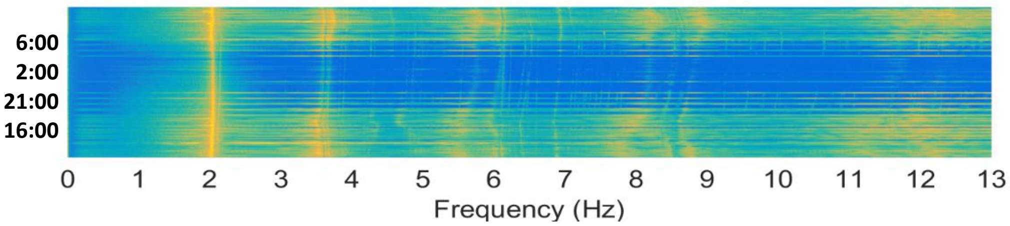

(b)

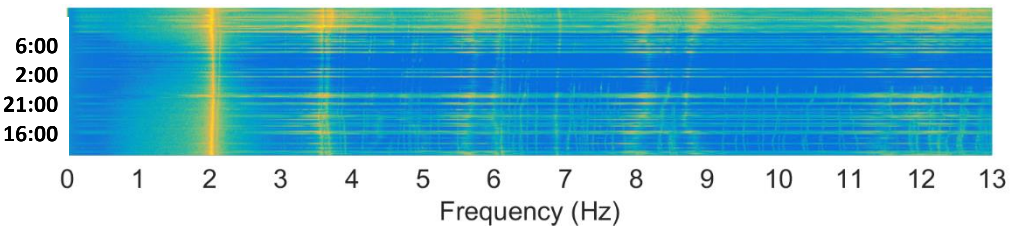

Figure 9. Illustration of the spectrogram of acceleration response for (a) weekday, (b) weekend.

Revised text:

Please look at Section 5 in the revise paper.

2. Reviewer II

"The manuscript deals with the automation of the operational modal analysis of a cable stayed bridge. The discussion of the proposed procedure, based in the NExT-ERA and SSI-CoV methods, is reported together with some results of experimental tests on a real scale structure."

2.1 Reviewer 2 - Comment 1

"The background literature and the related state of the art show some weak aspects that need to be improved."

Response:

The authors agree with the reviewer that the comprehensiveness of the background literature section needs to be enhanced. Therefore the author has improved the thoroughness of the literature review by including extra descriptions on the background of the algorithm which forms the basis of the proposed methodology in the manuscript. In particular, emphasises have been given to the initial literature work by Magalhaes et al. (2009) (http://dx.doi.org/10.1016/j.ymssp.2008.05.003) which utilizes hierarchical clustering algorithm in automated operational modal analysis. This work has been considered as an important background reference for the core of the automated algorithm proposed by the author. Furthermore, the work by Rainieri C and Fabbrocino G (http://dx.doi.org/10.1504/IJLCPE.2014.064099) has been included in the manuscript to provide stronger theoretical basis on the automation of the stabilization diagram analysis with the SSI algorithm. The details of these modifications on the literature review sections are specifically addressed in the individual comments provided to Reviewer 2-Comment 4 and Reviewer 2-Comment 8, where the relevant sections of the revised text are also provided.

2.2 Reviewer 2 - Comment 2

“The section #2 devoted to the presentation of OMA basics is too short and ineffective also in relation to the fragmentation into sub-sections made of a few lines. The same applies to some parts of the section #3, where the core of the work is discussed.”

Response:

Sections 2 and 3 in the original draft of the paper were significantly modified to resolve this issue.

Revised text:

The discrete-time representation of the equation of motion for a linear time-invariant dynamic system can be given by state-space formulation as (He and Fu 2001; Ewins 2000; Reynders and De Roeck 2008):

$$\begin{aligned} z(k+1) &= \boldsymbol{A}z(k) + w(k) \\ u(k) &= \boldsymbol{C}z(k) + v(k) \end{aligned}$$

where $\boldsymbol{A} \in \mathcal{R}^{n\times n}$ is the discrete-time state-space matrix, $z \in \mathcal{R}^{n}$ is the state vector, $w \in \mathcal{R}^{n}$ is the external input assumed to be a white Gaussian noise process, $u \in \mathcal{R}^{l}$ is the vector of measured responses, $\boldsymbol{C} \in \mathcal{R}^{l\times n}$ is the output matrix and $v \in \mathcal{R}^{l}$ is another white noise vector process representing the noise content of the measurements. k indicates the generic time step.

According to (Turner and Pretlove, 1998), for a bridge structure, it is valid to assume that the source of excitation as a result of passing traffic is a white Gaussian process. This can be attributed to the randomness in vehicle configurations i.e. different weights and axle configurations, randomness in arrival times, suspension system and road surface profile.

In this paper, SSI-Cov algorithm is adopted to identify a stochastic state-space model from output-only data. SSI-Cov algorithm is a time-domain parametric algorithm that deals with the stochastic realization problem to fit a state space model to the covariance of the responses driven by ambient excitation. SSI-Cov algorithm consists of the following steps: (1) computation of output covariance, $\widehat{\boldsymbol{R}}_{\boldsymbol{i}}$, (2) construction of the block Toeplitz matrix, $\boldsymbol{T}_{\boldsymbol{1}|\boldsymbol{i}}$, (3) decomposition of the Toeplitz matrix, (4) estimation of the controllability and observability matrices and (5) extraction of the modal parameters. These steps are elaborated below.

Let $\boldsymbol{Y}$, an $L \times Q$ matrix be the ambient vibration measurements for a structure, in which L is the total number of sensors and Q is the number of time steps in each set of sensor measurement as,

$$\boldsymbol{Y} = \begin{bmatrix} y_{1,1} & y_{1,2} & \cdots & y_{1,Q} \\ y_{2,1} & y_{2,2} & \cdots & y_{2,Q} \\ \vdots & \vdots & \vdots & \vdots \\ y_{L,1} & y_{L,2} & \cdots & y_{L,Q} \end{bmatrix}$$

The first step of SSI-Cov algorithm is the computation of output correlations $\widehat{\boldsymbol{R}}_{\boldsymbol{i}}$ according to,

$$\widehat{\boldsymbol{R}}_{\boldsymbol{i}} = \frac{1}{Q-i}\left[\boldsymbol{Y}_{(\boldsymbol{1}:\boldsymbol{Q}-\boldsymbol{i})}\right]\left[\boldsymbol{Y}_{(\boldsymbol{i}+\boldsymbol{1}:\boldsymbol{Q})}\right]^{\boldsymbol{T}},$$

where $\boldsymbol{Y}_{(\boldsymbol{1}:\boldsymbol{Q}-\boldsymbol{i})}$ is obtained from the matrix $\boldsymbol{Y}$ by removing the last i samples of data and $\boldsymbol{Y}_{(\boldsymbol{i}+\boldsymbol{1}:\boldsymbol{Q})}$ is obtained by removing the first i samples of data. The parameter i represents the time lag and it is required to be defined by the user. The calculated output correlations at different time lags are then combined to form a block Toeplitz matrix $\boldsymbol{T}_{\boldsymbol{1}|\boldsymbol{i}} \in \mathcal{R}^{Li\times Li}$ as,

$$\boldsymbol{T}_{\boldsymbol{1}|\boldsymbol{i}} = \begin{bmatrix} \widehat{\boldsymbol{R}}_{\boldsymbol{i}} & \widehat{\boldsymbol{R}}_{\boldsymbol{i}-\boldsymbol{1}} & \cdots & \widehat{\boldsymbol{R}}_{\boldsymbol{1}} \\ \widehat{\boldsymbol{R}}_{\boldsymbol{i}+\boldsymbol{1}} & \widehat{\boldsymbol{R}}_{\boldsymbol{i}} & \cdots & \widehat{\boldsymbol{R}}_{\boldsymbol{2}} \\ \vdots & \vdots & \vdots & \vdots \\ \widehat{\boldsymbol{R}}_{\boldsymbol{2i}-\boldsymbol{1}} & \widehat{\boldsymbol{R}}_{\boldsymbol{2i}-\boldsymbol{2}} & \cdots & \widehat{\boldsymbol{R}}_{\boldsymbol{i}} \end{bmatrix}$$

The block Toeplitz matrix $\boldsymbol{T}_{\boldsymbol{1}|\boldsymbol{i}}$ is decomposed via singular value decomposition as,

$$\left[\boldsymbol{T}_{\boldsymbol{1}|\boldsymbol{i}}\right] = U\Sigma V^T$$

where $U \in \mathcal{R}^{Li\times Li}$ and $V \in \mathcal{R}^{Li\times Li}$ are orthonormal matrices and $\Sigma \in \mathcal{R}^{Li\times Li}$ is a diagonal matrix containing the positive singular values in descending order. Let n be the number of none zero singular values of $\boldsymbol{T}_{\boldsymbol{1}|\boldsymbol{i}}$ which indicates the rank of Toeplitz matrix. The observability matrix $O_i \in \mathcal{R}^{Li\times n}$ and the controllability matrix $\Gamma_i \in \mathcal{R}^{n\times Li}$ can be defined as follows:

$$[O_i] = [U_1][\Sigma_1]^{\frac{1}{2}}$$

$$[\Gamma_i] = [\Sigma_1]^{\frac{1}{2}}[V_1]^T$$

where $U_1 \in \mathcal{R}^{Li\times n}$, $\Sigma_1 \in \mathcal{R}^{n\times n}$ and $V_1 \in \mathcal{R}^{Li\times n}$ are obtained by eliminating the zero singular values and the corresponding singular vectors.

The solution of the identification problem can be then obtained by,

$$[\boldsymbol{A}] = [\Sigma_1]^{-\frac{1}{2}} [U_1]^T [T_{2|i}][V_1] [\Sigma_1]^{-\frac{1}{2}}$$

$$[\boldsymbol{C}] = O_i(1{:}L)$$

where $\boldsymbol{T_{2|i}}$ is composed of covariances from lag 2 to $2i$ as,

$$[T_{2|i+1}] = \begin{bmatrix} [\hat{R}_{i+1}] & [\hat{R}_i] & \cdots & [\hat{R}_2] \\ [\hat{R}_{i+2}] & [\hat{R}_{i+1}] & \cdots & [\hat{R}_3] \\ \vdots & \vdots & \vdots & \vdots \\ [\hat{R}_{2i}] & [\hat{R}_{2i-1}] & \cdots & [\hat{R}_{i+1}] \end{bmatrix}$$

At this point the identification problem is theoretically solved. The modal parameters of the system can be extracted from the identified system description $[\boldsymbol{A}]$ and $[\boldsymbol{C}]$ as,

$$[\Psi]^{-1}[\boldsymbol{A}][\Psi] = [Z]$$

$$\lambda_r = \ln(Z_r)\,/\Delta t$$

$$\omega_r = \sqrt{(\lambda_r{}^R)^2 + (\lambda_r{}^I)^2}/2\pi$$

$$[\phi] = [\boldsymbol{C}] \times [\Psi]$$

$$\xi_r = \frac{|\lambda_r{}^R|}{\sqrt{(\lambda_r{}^R)^2 + (\lambda_r{}^I)^2}}$$

where Δt is the time step and Z_r is the r-th component of the matrix $[Z]$. $\lambda_r{}^R$ and $\lambda_r{}^I$ are, respectively, the real and imaginary components of λ_r. ξ_r is the damping factor for the r-th mode and $[\phi]$ is the matrix of mode shapes.

Revised text:

Please look at Section 2 in the revised paper.

2.3 Reviewer 2 - Comment 3

"The description of the experimental tests on the bridge needs to be improved; some weak aspects rely with the measurement chain and the resulting recorded acceleration time histories. Others rely with the presentation, discussion and interpretation of the results."

The authors absolutely agree with the reviewer that in the first draft of the paper the description of the experimental tests on the bridge and the measurement set-up have not been properly addressed. Significant effort has been made to resolve this issue in the revised paper. As mentioned earlier, since a limited number of data were available in the first draft of the paper, (the bridge had just been instrumented), no significant data analysis were carried out. In the revised version of the paper, the acceleration recordings were available 24/7 for about one month which provided us with this opportunity to perform further analyses in order to investigate the performance of the method.

Details on the experimental tests, measurement set-up and the resulting time histories have been elaborated and can be found in the answers provided to Comment 5 of Reviewer 2. Also, please look at Sections 4 and 5 in the revised paper. Additionally, significant effort was made to ensure the proper interpretation and presentation of the results as can be seen in Sections 4 and 5 of the revised paper.

2.4 Reviewer 2 - Comment 4

"In order to support the authors in the revision process, a list of comments on specific aspects are reported below."

- It has been already observed that the background literature does not properly reflect available studies and achievements on the subject. In particular, as paper #17 is considered, it is worth

noting that the most significant achievements on the subject are reported elsewhere (Magalhaes, 2009) http://dx.doi.org/10.1016/j.ymssp.2008.05.003; thus, reference #17 has to be modified accordingly.

Response:

The authors agree with the reviewer that reference #17 in the original manuscript demonstrates a lack of focus in the field of automated OMA. Thus reference #17 is replaced by the suggested paper by Magalhaes et al. (2009) (http://dx.doi.org/10.1016/j.ymssp.2008.05.003) and the relevant sections in the text are modified in accordance to this work. The suggested paper is a pioneer study for efficiently implementing the concept of hierarchical clustering for automatic OMA with SSI-Cov algorithm and the corresponding contribution is articulated in the revised text.

Revised text:

In hierarchical clustering, each identified mode is linked based on the similarities in specific attributes such as natural frequency and mode shapes. The core concept of the automated algorithm with hierarchical clustering is that an automatic threshold is defined so that modes belong to the same set are separated into individual clusters and thus identified. There have been prior applications of hierarchical clustering on OMA with the SSI-Cov method where the algorithm has been demonstrated to be efficient and effective in automatic modal identification (Reynders et al. 2012; Magalhaes et al. 2009).

- Reference to a set of doctoral theses to support the statement appears to be not appropriate - see page 2, line 20 - and to be reductive of the research carried out on the subject. Reference #19 can be removed, eventually substituted by the book quoted as #10; journal papers like http://dx.doi.org/10.1016/j.ymssp.2015.01.019 and:

http://dx.doi.org/10.1155/2014/845106 should be considered. Their reference to a different approach to the automated modal analysis based on the concept of the hybridization of the traditional identification techniques fulfills the framework to the interested reader.

Response:

The authors strongly agree with the reviewer's comment that referencing to the doctoral theses #19 and #20 are ineffective as the focuses of the theses are very much irrelevant to the development of automatic OMA algorithms. In conjunction with the comments from reviewer 3, reference #19 was replaced by a more relevant study on automated OMA and damage detection by Magalhaes et al. (2012) (doi: 10.1016/j.ymssp.2011.06.011). This work highlights the capabilities of utilizing automated OMA algorithms for modal tracking and damage identification over a 2-year period with the utilization of the Covariance driven Stochastic Subspace identification (SSI-Cov) method. Comprehensive demonstration on the current progress on automated OMA is clearly revealed within this paper in support of the algorithm outlined in the authors' manuscript. Thus, the following revised text in Section 1 has been added to articulate the contribution of this work by Magalhaes et al. (2012).

Revised text:

These methods are widely used for vibration-based SHM (Rainieri and Fabbrocino 2015; Magalhaes et al. 2012). The Covariance driven stochastic Subspace Identification (SSI-Cov) method was applied by Magalhaes et al. (2012) for monitoring the damage conditions of a bridge based on the identified modal characteristics over a 2-year period. The results demonstrate clear relationships between the damage states of the bridge and frequency shifts of the dominant vibration modes.

- Reference to thesis #19 at page 3, line 3 seems to be ineffective. In combination with the book ref. #10 it is recommended to consider the following journal papers more focused on the concepts recalled in the text: http://dx.doi.org/10.3233/SAV-2010-0534 and:

http://dx.doi.org/10.1504/IJLCPE.2014.064099

Response:

The authors agree with the reviewer's comment that referencing to thesis #19 is irrelevant to the discussion on the system order selection for stabilization diagram. Therefore, this reference was eliminated and the paper by Rainieri C and Fabbrocino G (http://dx.doi.org/10.1504/IJLCPE.2014.064099) was included, as this work deals with much greater relevance on the relationships between the model order and accuracy of the identification results using SSI.

Revised text:

Both ERA and SSI are expressed based on the state-space model, where the maximum number of modes that can be identified is determined by the selected model order n which governs the size of the state-space matrix (Rainieri and Fabbrocino 2014a). Since the true model order is unknown and inappropriate model order selection can generate biased identification results (Rainieri and Fabbrocino 2014b), the selected model order is normally over-specified to ensure a complete coverage for all the real structural modes. However, spurious mathematical modes are also introduced as a result of this over-specification; thus, stabilization procedure is commonly adopted to identify the physical modes among all the identified modes. In contrast to physical modes, mathematical modes are not identified in a consistent way. The purpose of stabilization is to identify the stable modes with identical modal properties demonstrated through consecutive model orders. (Rainieri and Fabbrocino 2014a).

-This referee agrees with the statement by the authors reported at page 3, line 7-8-9. However, the current form of the text does not take into account available experiences reported in the technical literature, see for instance:

http://dx.doi.org/10.1016/j.engstruct.2011.10.001 . Particularly, the mentioned paper seems to be able to support the set of criteria discussed by the authors to discriminate between physical and 'virtual' modal parameters (see also page 5, line 9-10).

Response:

The authors agree with the reviewer's comment that on page 3, line 7-8-9, inadequate articulation is presented on the current available research for fully automated OMA techniques. However, the author's manuscript focuses on the automation of time-domain-based OMA method such as SSI-Cov algorithm where the elimination of any manual tunning steps in the process of clearing the stabilization diagram is critical for determining the performance of the automated algorithm. The suggested research article by (Rainieri C et al. 2012) (http://dx.doi.org/10.1016/j.engstruct.2011.10.001) seems to provide a comparison of different automated OMA techniques in both time and frequency domains and highlights the superiority in the performance of the frequency-domain LEONIDA method. Since stabilization diagram is not implemented in LEONIDA or other similar frequency-domain OMA techniques, the authors argue that the relevance of this work is not so high to the current manuscript. The authors also agree that the suggested article (Rainieri C et al. 2012) does provide some necessary basics for supporting the set of criteria applied in the initial stage of eliminating the spurious modes from the stabilization diagram (on page 5, line 9-10). However, this work does not include sufficient details on the rationale behind the design and selection of the set of criteria whereas a clearer basis can be obtained from the currently cited paper by Reynders et al. (2012) (http://dx.doi.org/10.1016/j.ymssp.2012.01.007).

2.5 Reviewer 2 - Comment 5

"Description of the measurement chain adopted during the experimental campaign is primarily focused on the commercial designation of the components. This circumstance - apart from any publisher's policy issues - is not satisfactory from the technical standpoint. The authors, instead of the commercial designation are recommended to report in detail the technical features and characteristics of the acquisition system and sensors. In particular, presence of anti-aliasing filters, sensitivity and full-range of the accelerometers, their technology and suitability for modal analysis - noise levels vs recorded accelerations -. On these specific aspects, the analysis of the records should confirm the acceptance of the measures in view of OMA processing."

Response:

The authors agree with the reviewer that the technical features and characteristics of the instrumentation/ measurement and experimental campaign might not be adequately addressed in the first draft. In the revised version, this issue was resolved and the commercial designation of the hardware was minimized.

Sensor array

The measurement grid for the dynamic test consists of 25 synchronized accelerometers to measure the acceleration responses of the deck, cables and the mast. These sensors were permanently installed on the bridge in order to monitor the dynamic behavior of the bridge and to identify the modal parameters. It is worth noting that during the instrumentation, the traffic lanes in Great Western Highway under the bridge were partially closed; thus, no roving of the sensors were considered due to the access limitations. 24 uni-axial sensors were placed under the deck at the intersection of the girders and floor beams to measure the vertical acceleration of the bridge, (see Figure 10). These sensors are low noise accelerometers with model number 2210-002 manufactured by Silicon Design, Inc (2010). The 2210-002 is a sensor that incorporates a 1210L micro-machined capacitive accelerometer. This model can detect accelerations within the range of ± 2 g with an output noise of 10 μg/√Hz and sensitivity of 2,000 mV/g.

The under deck accelerometers were adhered to the lightly sanded and cleaned paint using adhesive tape and covered with elastic joint sealant. All installations were coated with paint to reduce corrosion and improve the visual amenity of the installation. Figure 11 shows one of these sensors mounted under the girder before coating.

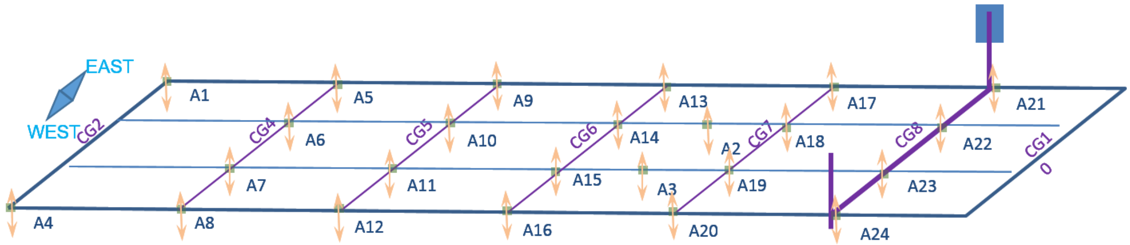

Figure 10. The accelerometer array on the deck.

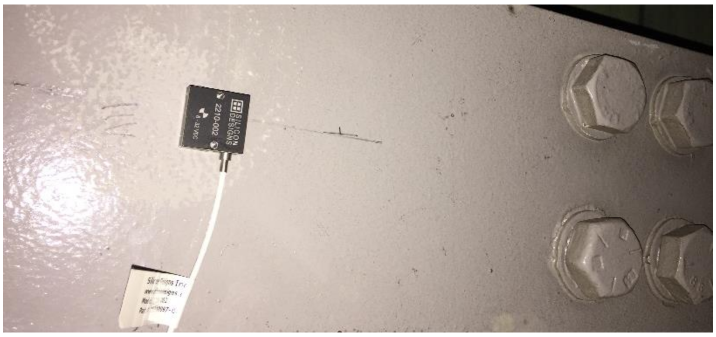

Figure 11. Illustration of the attached uni-axial accelerometer under the girder.

Another four 2210-002 uni-axial accelerometers were mounted on the cables on the eastern side of the bridge. These sensors measure the acceleration response of the cables in the vertical plane orthogonal to the line of the stay. In addition, one tri-axial accelerometer (Silicon Designs 2460-002) was installed on top of the mast to measure the vertical, lateral and longitudinal acceleration responses of the tower.

Data acquisition and measurement set up

The signal conditioning and data logging software consist of an embedded PC and HBM Quantum-X data logger to record data. This system provides an integrated and reliable device to log high quality data with 24bit resolution with bandwidth capability of 0 to 3 kHz. This hardware combines instrument excitation, voltage regulation, digitization, anti-aliasing filters and data logging. The logging software is Catman. The software collects all channels at a default sample rate of 600 Hz with an anti-aliasing filter. The 3 dB cut-off frequency of the filter is 100 Hz and it is a fourth order Bessel low-pass filter with details shown in Figure 12. The selection of this high sampling frequency in the system is solely to meet the requirements of other research activities on this bridge i.e. Bridge-Weigh-in-Motion (BWIM) and tensor analysis. It should be noted that a dense array of strain gauges, timely synchronized with the accelerometers, have been installed under the deck in this bridge which is out of the scope of this paper (Kalhori et al. 2017). Moreover, according to the initial finite element modeling some modes around 60 Hz were observed in this bridge, and this high sampling rate was selected to make accurate identification of these high frequency modes possible. However, in this study, the frequency range of interest is only up to 13 Hz and no effort has been made to extract the higher frequency modes.

Decimal sample rates and digital low pass filter, type Bessel 4th order

Typ	-1dB (Hz)	-3dB (Hz)	-20dB (Hz)	Phase delay*) (ms)	Rise time (ms)	Overshoot (%)	Rate (Hz)
Bessel	1,203	2,000	3,830	0.113	0.189	2.10	20,000
	596	1,000	2,494	0.256	0.355	1.0	20,000
	298	502	1,278	0.581	0.701	0.9	20,000
	119	200	509	1.56	1.76	0.9	20,000
	59	100	254	3.21	3.51	0.9	20,000
	29.6	49.9	127.1	6.50	7.01	0.9	20,000
	11.8	20.0	50.8	16.4	17.6	0.9	20,000
	5.9	10.0	25.4	32.9	35.1	0.9	20,000
	2.96	4.99	12.70	69.0	70.1	0.9	10,000
	1.18	2.00	5.08	168	176	0.9	10,000
	0.59	1.00	2.54	333	351	0.9	5,000
	0.295	0.498	1.271	663	701	0.9	1,000
	0.118	0.200	0.508	1,660	1,760	0.9	1,000
	0.059	0.100	0.254	3,300	3,510	0.9	500
	0.0295	0.0498	0.1271	6,620	7,010	0.9	100
	0.0118	0.0200	0.0508	16,500	17,600	0.9	100
	0.0059	0.0100	0.0254	33,000	35,100	0.9	50

*) The analog-to-digital converter's delay time is 128 μs for all data rates and has not been accounted for in the "Phase delay" column!
The anti-aliasing filter's delay time (160 μs) is not accounted for as well. Hence. 288 μs need to be added to the "Phase delay".

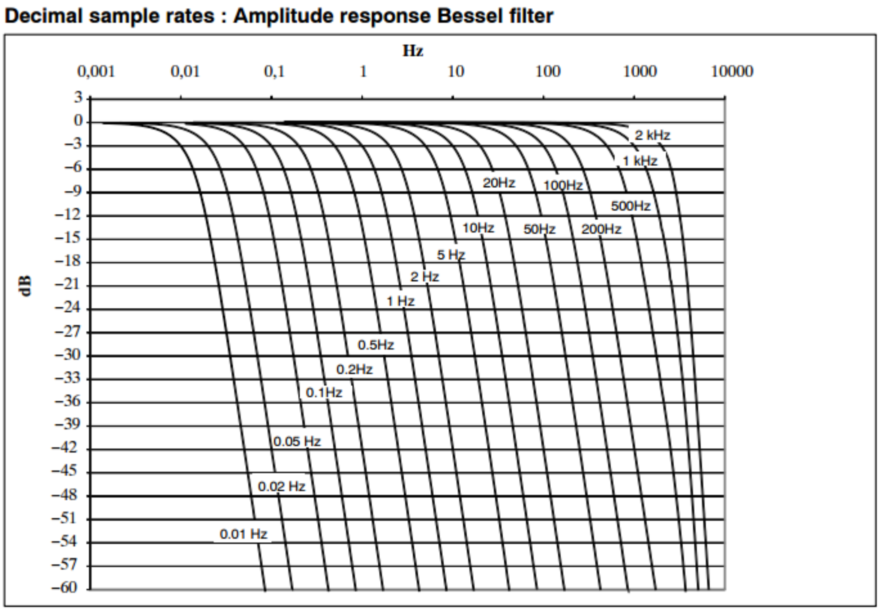

Figure 12. Details of the Bessel low-pass filter.

For the purpose of identifying the modal properties of the bridge under operational conditions and consequently building time histories of modal parameters, the dynamic monitoring system continuously records the vibration response of the bridge and it produces a file with acceleration time series per 10 minutes. A total number of 144 files is generated per day. 360,000 samples are acquired for each channel for a 10-minute-long acceleration signal. The measured data are continuously transferred over a 4G cellular network to the database.

Figure 13 (a) illustrates typical acceleration time signal obtained from a 10-minute file from channel A7. Light traffic flow over the bridge is evident from this figure. Typical ambient part of the response, once no vehicle is traveling over the bridge i.e. the first 16.67 seconds (≈ 0.3 min) is illustrated in Figure 13 (b). As seen, the vibration of the bridge with its first natural frequency is quite obvious in the acceleration response.

22 days of monitoring data, continuously acquired from the 1st of November until the 22nd of November 2016 are used in this paper for the purpose of operational modal analysis. This selection was only made due to the availability of data in this time period. For each day, three files were considered. The files were selected from different times within 24 hours including midnight, and rush traffic hours. This provides a total number of 66 10-minute-files for our investigations.

(a) (b)

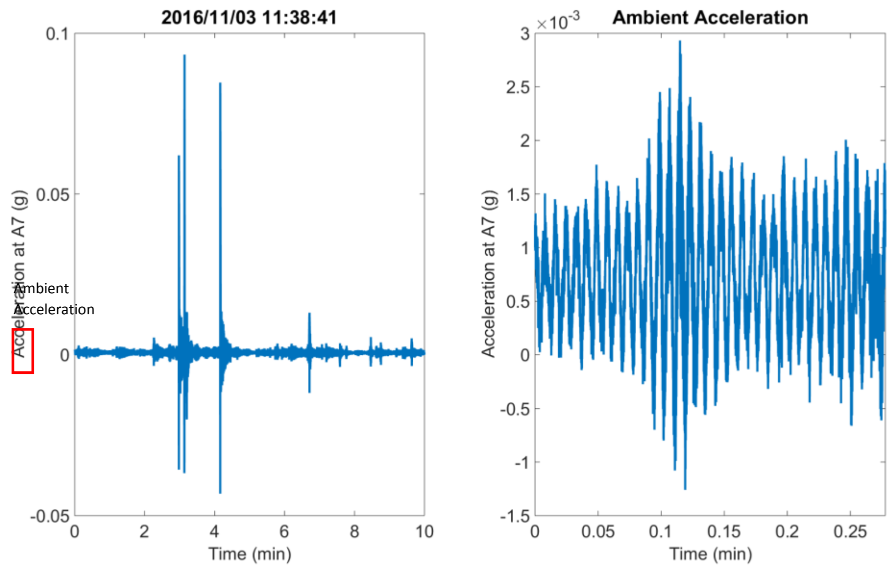

Figure 13. (a) Typical 10-minutes acceleration time history including response as a result of passing traffic, (b) typical ambient part of the response while there is no vehicle on the bridge.

Preprocessing and parameters of the algorithm

The analysis of the experimental data involved initial pre-processing operations to eliminate the offset and to ensure there is no spike or unreasonable noise in the signals. The entire 10-minute acceleration response was adopted for the analysis. This includes 360,000 data points from each channel. A Hanning window was applied to the time signals to minimize leakage. Parameter i, was selected to be 100 and a maximum model order of 160 was considered to construct the stabilization diagram.

In a separate study, the time signals were decimated with a factor of 5 which resulted in 72,000 samples from each channel. Decimation of the signals can help to enhance the ability of the estimation process in identification of the lower frequency modes. However, it was realized that the results with and without decimation are quite similar, hence, the results obtained from the original time signals were only presented.

Revised text:

Please look at Section 4 in the revised paper.

2.6 Reviewer 2 - Comment 6

"The duration of the acceleration records represents another key issue of the paper. Since the authors claim an automated identification of the modal parameters, it is really surprising that a so short time record (10 min) is referred. Apart from the reliability of the estimates related to this parameter, it is worth noting that the capabilities of an automated procedure should be assessed by means of a validation of the process in time. In other words, the authors are invited to better explain if the procedure is aimed at solving the problem of a single test or to be the core of long-term vibration based structural health monitoring system. If the latter is the case, stability accuracy and frequency of failed/missed identifications should be considered and discussed in the text."

Response:

With all respect, the authors believe the duration of 10 minutes measurement is not too short as it provides 360,000 samples for each channel; also according to the literature on operational modal analysis of bridge structures, the duration of 10 minutes seems to be quite comparable. According to (Cantieni. 2005) the length of time window should be 1000-2000 times the period of the structure's fundamental mode; in our case, this number is 1200 which satisfies the recommended range. In the previously published works, a duration of three minutes with sampling frequency of 128 Hz has been adopted in (Whelan et al. 2009) to identify modal parameters of a highway bridge. In a separate study by (Siringoringo and Fujino. 2008) the duration of 15 minutes has been considered for system identification of a suspension bridge from ambient vibration response. In another study, vibration analysis of a cable-stayed arch bridge has been performed by analyzing 16-minute vibration response under ambient excitation (Galvín and Domínguez. 2007). Finally, 250 seconds vibration response of a cable-stayed bridge subject to wind-induced ambient vibration has been considered in (He et al. 2008) to extract the modal parameters. Hence, according to the previously reported research works on OMA for bridge structures, it is obvious that our data acquisition setting i.e. sampling frequency of 600 Hz and duration of 10 minutes is quite reasonable.

The authors absolutely agree with the reviewer that the capability of the method has not been well assessed which was mainly due to the lack of data while the first draft of the paper was prepared. The aim of the procedure is not a single test whereas it is a long-term vibration-based structural health monitoring system. This has been elaborated earlier in this report and the reviewer is kindly asked to look at the responses provided to: Reviewer 1 - Comment 4.

2.7 Reviewer 2 - Comment 7

"The results provided in Table 2, 3 & 4 show some criticism that need careful consideration. Unfortunately, the format of Figure 5 & 6, the graphical representation of the mode shapes (Fig. 7) do not enable the interested reader - at the moment this reviewer - to carry out a verification of the values collected in the above reported tables. A more detailed scaling of the frequency axis of the stabilization diagrams, a different scale and format of the modal shape plots could be more effective and significant. In principle, it is opinion of this reviewer that some words should be dedicated to the role of the cables and their dynamic interaction with the identification of the deck. This circumstance is by far more relevant since the bandwidth of the modes reported in Table 2 & 3 is not narrow. Then, the motivation of a so large number of identified modes should be provided, especially in a case like the one reported in the manuscript were missed identification often affects the primary modes (see Table 4, for instance)."

Response:

First of all, the authors accept that the presentation and discussion of the results in the first draft of the paper had a lot of problems and needed significant improvements. In the revised paper, all the analyses have been done from the scratch on new datasets that were not available while the first draft of the paper was prepared. Details about all the changes made in the revised paper on data acquisition, measurement set-up, data analysis and results have been elaborated in responses to: Reviewer 1 - Comment 1, Reviewer 1 - Comment 4 and Reviewer 2 - Comment 5 which answer all the comments raised by the reviewer in this question.

The reviewer is absolutely right. Basically, the cable-stayed bridges are low-damped structures experiencing high amplitude vibrations; the dynamic coupling between the cables and the bridge deck is an important and a very complex phenomenon which corresponds to occurrence of internal resonances between the global (deck-dominant) and local (cable-dominant) modes. This coupling might involve lateral bending and torsional motions of the deck together with the vertical and swinging motions of the cables. Although, there is not yet a complete knowledge of the mechanism behind this strong interaction, several potential causes have been considered such as wind/rain-induced excitations. According to our literature, the dynamic interaction between the cables and the deck/tower system associates with the appearance of several closely-spaced modes, involving different cable movements, but similar configurations of the deck vibration; this phenomenon can be clearly seen in the mode shapes presented in Figure 6 (Abdel-Ghaffar and Khalifa, 1991, Caetano et al. 2000, Caetano et al. 2008, Larose et al. 2003).

2.8 Reviewer 2 - Comment 8

"As damping estimates are concerned, see page 15 line 17-19, it is worth checking and referring to the paper http://dx.doi.org/10.3233/SAV-2010-0534 that appears to fit very well the context recalled by the authors."

Response:

The authors agree with the reviewer's comment that the suggested paper by Rainieri et al. (2010) (http://dx.doi.org/10.3233/SAV-2010-0534) is closely relevant to the context of page 15 line 17-19. This work provides thorough explanations on the high scatterings and variations observed in the identified damping ratios for identical modes. Thus, the following revised texts are added for articulating the relevance between these findings by Rainieri et al. and the identification results presented in this manuscript.

Revised text:

Rainieri et al. (2010) suggested that the presence of inherent limitations or inaccuracies of data processing methodologies can both lead towards high variations in damping ratio estimates. Inappropriate selection of modal order for the stabilization diagram may also enlarge the scattering of damping ratio for each identified mode.

2.9 Reviewer 2 - Comment 9

“A detailed discussion of the outcomes of the AUTOMAC checks is recommended. Too high appear some values off the main diagonal in the absence of comprehensive analysis of the results (see the above comments).”

First of all, the authors would like to emphasize that the procedures for calculating the MAC values in the first draft of the paper (please see Figure 7 in the first draft) has not been correctly addressed. The reason is that the MAC has been calculated using the modes identified from a single dataset only and it is evident that all the diagonal members have to be 1 which does not add any value. This problem has been resolved in the revised version as elaborated in response to Reviewer 1 - Comment 4.

2.10 Reviewer 2 - Comment 10

“It is not really clear the motivation of the missed manual identification reported in Table 2, 3 and 4. Authors should well explain this circumstance that could be again strictly related to the answers to comments #5 and #6.”

Response:

With regards to the comment about the missed modes presented in Table 2, the reviewer is kindly asked to read through the response to Reviewer 1-Comment 3. Regarding Tables 3 and 4, the reviewer is also kindly asked to look at the response to Reviewer 1 - Comment 4.

2.11 Reviewer 2 - Comment 11

"Plots of the recorded acceleration time histories refer to different time durations (see comment #6) and miss the units on the vertical axis. On this subject, the authors should discuss in detail the motivation of the 600 Hz sampling frequency and the adoption of eventual data pre-treatment before OMA processing (trend removal, decimation, windowing and so on)."

Response:

The authors have significantly modified the plots of acceleration responses and the units have been included.

The selection of this high sampling frequency in the system is solely to meet the requirements of other research activities on this bridge i.e. Bridge-Weigh-in-Motion (BWIM) and tensor analysis. It should be noted that a dense array of strain gauges, timely synchronized with the accelerometers, have been installed under the deck in this bridge which is out of the scope of this paper. Moreover, according to the initial finite element modeling some modes around 60 Hz were observed in this bridge, and this high sampling rate was selected to make accurate identification of these high frequency modes possible. However, in this study, the frequency range of interest is up to 13 Hz and no effort has been made to extract the higher frequency modes.

Please look at the response provided to Reviewer 2 - Comment 5 for all the details related to the pre-processing of data.

2.12 Reviewer 2 - Comment 12

"A more detailed description of the dynamic tests carried out in the presence of vehicle crossing the bridge is recommended. Some basic information about the vehicles and their approach to the bridge (position, trajectories, crossing frequency, number of vehicle in the crossing line and so on). This should provide to the reader any useful information to explain the missed identification of some primary flexural modes of the deck. The above comments prevent the publication of the paper in the present form. Major revisions are consequently required."

Response:

Please kindly look at the response provided to Reviewer 1 - Comment 4.

3. Reviewer III

"The paper deals with the development of an automated Operational Modal Analysis (OMA) procedure to be used for modal based damage detection of civil structures. The originality of the proposed method is limited. Discussion and validation are not sufficient. I recommend to significantly revise the paper in order to make it eligible for publication. The following comments can provide guidance to strengthen the manuscript."

3.1 Reviewer 3 - Comment 1

"The literature review is sufficient but it includes some inappropriate references. Moreover, it should be rearranged to highlight the novelty of the proposed method, which appears very similar to the one described in Ref. [16]. About the references, Ref. [9] does not deal with automated OMA: you can replace it (and Ref. [17] on pag. 15 line 18) with the following: Rainieri C., Fabbrocino G. Development and validation of an automated operational modal analysis algorithm for vibration-based monitoring and tensile load estimation. Mechanical Systems and Signal Processing, 60-61, 512-534, 2015. Moreover, I recommend to replace Ref. [19] and [20], which are just Ph.D. theses, with peer reviewed papers or books: for instance, you can replace Ref. [19] with Magalhaes F., Cunha A., Caetano E. Vibration based structural health monitoring of an arch bridge: from automated OMA to damage detection, Mechanical Systems and Signal Processing, 28, 212-228, 2012, and Ref. [20] with Farrar C.R., Worden K. Structural Health Monitoring: A Machine Learning Perspective, John Wiley & Sons Ltd., Chichester, UK, 2013. Finally, I recommend to cite the following original paper: Magalhaes F., Cunha A., Caetano E. Online automatic identification of the modal parameters of a long span arch bridge, Mechanical Systems and Signal Processing, 23, 316-329, 2009, instead of Ref. [17], since that is definitely more appropriate and relevant to the discussion than Ref. [17]."

Response:

The authors agree with the reviewer's comment that certain references are inappropriate for supporting the literature review. Regarding the references, reference #9 was replaced by Rainieri C. and Fabbrocino G., 2015. The work by Rainieri and Fabbrocino suits well in the context of this manuscript as it focuses on the implementation of SSI-Cov algorithm for automated modal identification with the implementation of clustering approaches. The authors also agree with the reviewer's comment that referencing to the PhD theses #19 and #20 are ineffective as the focuses of the thesis are very much irrelevant from the development of automatic OMA algorithms. In conjunction with the comments from reviewer 2, reference #19 was replaced by a more relevant study on automated OMA and damage detection by Magalhaes et al. (2012) (doi: 10.1016/j.ymssp.2011.06.011). This work highlights the capabilities of utilizing automated OMA algorithms for mode tracking and damage identification over a 2-year period with the utilization of the Covariance driven Stochastic Subspace identification (SSI-Cov) method. Comprehensive demonstration on the current progress on automated OMA is clearly revealed within this paper in support of the algorithm outlined in the authors' manuscript. Thus the following revised text has been added to articulate the contribution of this work by Magalhaes et al. 2012.

Revised text:

These methods are widely used for vibration-based SHM (Rainieri and Fabbrocino 2015; Magalhaes et al. 2012). The Covariance driven stochastic Subspace Identification (SSI-Cov) method was applied by Magalhaes et al. (2012) for monitoring the damage conditions of a bridge based on the identified modal characteristics over a 2-year period. The results demonstrate clear relationships between the damage states of the bridge and frequency shifts of the dominant vibration modes.

Response (continued):

The original doctoral thesis cited in reference #20 is removed due to its low relevance with automated OMA. The author has considered replacing this reference by the following recommended book; Farrar C.R., Worden K. Structural Health Monitoring: A Machine Learning Perspective, John Wiley & Sons Ltd., Chichester, UK, 2013. This work introduces the applicability of widely applied machine learning approaches in the context of structural health monitoring. However, the primary focus of the authors' manuscript is the development and application of an automatic algorithm for OMA, which is not closely relevant to the book. Therefore the original reference #20 was deleted from the manuscript.

The authors agree with the reviewer that reference #17 in the original manuscript demonstrates a lack of focus in the field of automated OMA. Thus, reference #17 is replaced by the suggested paper; (Magalhaes F., Cunha A., Caetano E. Online automatic identification of the modal parameters of a long span arch bridge, Mechanical Systems and Signal Processing, 23, 316-329, 2009). The relevant sections in the text are modified in accordance to this work. This paper is a pioneer study for efficiently implementing the concept of hierarchical clustering for automatic OMA identification with SSI-Cov algorithm and the corresponding contribution is articulated in the following additional paragraph in the revised text.

Revised text:

In hierarchical clustering, each identified mode is linked based on the similarities in specific attributes such as natural frequency and mode shapes. The core concept of the automated algorithm with hierarchical clustering is that an automatic threshold is defined so that modes belong to the same set are separated into individual clusters and thus identified. There have been prior applications of hierarchical clustering on OMA with the SSI-Cov method where the algorithm has been demonstrated as efficient and effective in automatic modal identification (Reynders et al. 2012; Magalhaes et al. 2009).

3.2 Reviewer 3 - Comment 2

"Section 2 is definitely useless in its current form: it should be expanded in order to include relevant information (for instance, it should discuss how the modal properties are finally estimated). Moreover, SSI-Cov and NExT-ERA are basically the same method, as remarked by several Authors in the literature. Thus, I recommend presenting the theoretical background of SSI-Cov only, and removing the fictitious distinction between the two methods. Finally, Equation (1) is inappropriate for two reasons: 1) it refers to input-output modal analysis instead of OMA; 2) it does not include the direct transmission matrix, even if it should be there taking into account the content of Section 4."

Response:

In the revised paper, Section 2 was significantly improved and the detailed procedure of modal parameters identification was elaborated.

With all respect, the authors do not agree with the reviewers' comment that SSI-Cov and NExT-ERA are the same. Basically, the development of OMA in the time domain can be classified into three main approaches: (1) natural excitation technique (NExT) based approaches, (2) stochastic subspace identification (SSI) based approaches and (3) autoregressive moving average (ARMA) based approaches. In the original draft of the paper the first two approaches have been adopted. The basic idea of NExT is that the cross- correlation function of two random responses of the structure that result from an unknown white noise excitation can be expressed as a summation of decaying sinusoids. These sinusoids have the same characteristics as the system's impulse response function (IRF). Hence, time domain modal identification techniques which are typically applied to IRF (i.e. Ibrahim time domain, eigenvalue realization algorithm, polyreference complex exponential), can be applied to these cross-correlation functions to estimate modal parameters (Karbhari & Ansari, 2009). In this study NExT was paired with eigenvalue realization algorithm (ERA). The variables in this procedure include the shape of the Hankel matrices (number of lags used) and the number of reference channels (Brownjohn, Magalhaes, Caetano, & Cunha, 2010). The stochastic subspace identification (SSI) based methods are based on the concept of system realization to identify the system matrices. In the covariance-driven stochastic subspace identification method (SSI-Cov), adopted in this study, stochastic realization is calculated by performing the decomposition of the covariance matrix of the response instead of the decomposition of IRF. Thus this procedure is similar to NExT-ERA method, however, they are not the same (Karbhari & Ansari, 2009). The input parameters are also different with the ones in ERA. SSI-Cov algorithm requires the user to choose an important setting which is the number of lines of the covariance function to build the Toeplitz matrix (Brownjohn & Carden, 2007). According to the above, although two methods are similar, they are not the same and it is expected that application of these two methods on the same dataset provides different results as also evident from the literature; for instance, in (Brownjohn, Magalhaes, Caetano, & Cunha, 2010) a maximum difference of 8.4% and 2.6% has been, respectively, reported for the identified vertical and torsional modes and the lateral modes obtained from these two approaches. However, the authors decided to eliminate the NExT-ERA from the revised paper and only focused on SSI-Cov algorithm.

As for the Equation (1), it was slightly modified and the current form is as follows,

$$\begin{aligned} z(k+1) &= \boldsymbol{A}z(k) + w(k) \\ u(k) &= \boldsymbol{C}z(k) + v(k) \end{aligned}$$

This equation describes an output-only dynamic system using a stochastic state-space model (Rainieri, C. et al. 2007, Peeters and Roeck, 1999, Hermans and Auweraer, 1999). Basically, the idea of OMA is to use output-only or stochastic system identification algorithms, in which the unknown ambient loading conditions are modelled as stochastic quantities with unknown parameters but with known behaviour (for instance, white noise time series with zero mean and unknown covariances). The eigenvalues of the state transition matrix $\boldsymbol{A}$ characterize the dynamic behaviour of a physical system. By computing the state transition matrix $\boldsymbol{A}$ and measurement matrix $\boldsymbol{C}$, it is possible to obtain the modal parameters of the system. The theoretical problem considered here is the estimation of the modal parameters from a given discrete-time output vector $\{u\}$ which is modelled by a discrete-time stochastic state-space as shown in Equation (1). Please also look at the response provided to Reviewer 2 - Comment 2.

Revised text:

3.3 Reviewer 3 - Comment 3

"The method presented in Section 3 basically resembles the one described in Ref. [16]. The novelty is limited to the approach to select the threshold in hierarchical clustering. The discussion of the method is obscure in several parts. For instance, the MEL index defined by Equation (10) is based on the input matrix B, which cannot be computed in the OMA framework. In addition, when the second application of k-means (right after the hierarchical clustering) is discussed, even if k is set equal to 2, the Authors declare that "a number of additional empty sets are added". What is the role of these empty sets? Is the number of identified clusters larger than 2? Lines 18-20 on page 10 seem to confirm that k-means clustering with k>2 is applied. Please, add a flowchart of the proposed algorithm."

Please look at the response provided to the Reviewer 1- Comments 1, 3 and 4 for more details on the new analyses performed.

In the covariance driven stochastic subspace identification algorithm (SSI-Cov) utilized in this work, the input matrix $[B]$ is equivalent to the state-output covariance matrix $[G]$ represented in the following reversed controllability matrix according to Rainieri and Fabbrocino (2014a).

$$[\Gamma_i] = \left[[A]^{i-1}[G] \ \ \cdots \ \ [A][G] \ \ [G]\right]$$

This reversed controllability matrix along with the observability matrix form the block Toeplitz matrix $[T_{1|i}]$ can be identified directly based on the output vibration responses using SSI-Cov algorithm, with the details shown in Chapter 4.5.3.1 by Rainieri and Fabbrocino (2014a). In addition, the block Toeplitz matrix can be represented by the following equations based on singular value decomposition:

$$[T_{1|i}] = [O_i][\Gamma_i] = [U_1][\Sigma_1][V_1]^T$$

$$[O_i] = [U_1][\Sigma_1]^{1/2}$$

$$[\Gamma_i] = [\Sigma_1]^{1/2}[V_1]^T$$

The matrix $[G]$ or matrix $[B]$ is the last l columns of $[\Gamma_i]$, where l is the number of sensor measurements available from the vibration responses. For more clarification, please also look at the response provided to Reviewer 2 - Comment 2.

The authors agree that the descriptions in lines 18-20 on page 10 of the original manuscript are misleading. During the final stage of the automatic algorithm, the *k*-means clustering applied; the number of clusters is always equal to 2 where one cluster represents the real modes and the other cluster represents the spurious modes. When the authors wrote "a number of additional empty sets are added", the authors mean that the empty sets are added to the overall sample before the *k*-means clustering is applied. For example, if four clusters are to be analyzed by the *k*-means clustering which contain 100, 75, 55 and 25 poles, respectively, the number of empty clusters added are equal to the number of clusters with poles greater than one fifth of the largest cluster so that four empty sets are added. Thus there will be a total of eight clusters or sets where four of them will be empty before the *k*-means clustering is applied to determine the final identified clusters that represent real modes. The purpose of adding these empty sets is to avoid any physical (real) modes being accidentally deleted during the *k*-means clustering. For the above example, assume that the first three clusters with 100, 75 and 55 poles represent real modes and the final cluster with 25 poles represents spurious mode. If no empty set is added, the *k*-means clustering will classify the first two clusters with 100 and 75 poles as real modes however, the third real mode represented by the cluster with 55 poles is misclassified as spurious mode. On the other hand, if four empty sets are added, then the *k*-means clustering will identify the first three clusters with 100, 75 and 55 poles as real and the other ones as spurious so that the results are the same as predicted. Therefore it is clearly demonstrated that with the addition of the empty sets, the performance of the algorithm is enhanced. A flowchart for the proposed algorithm is shown in the following figure:

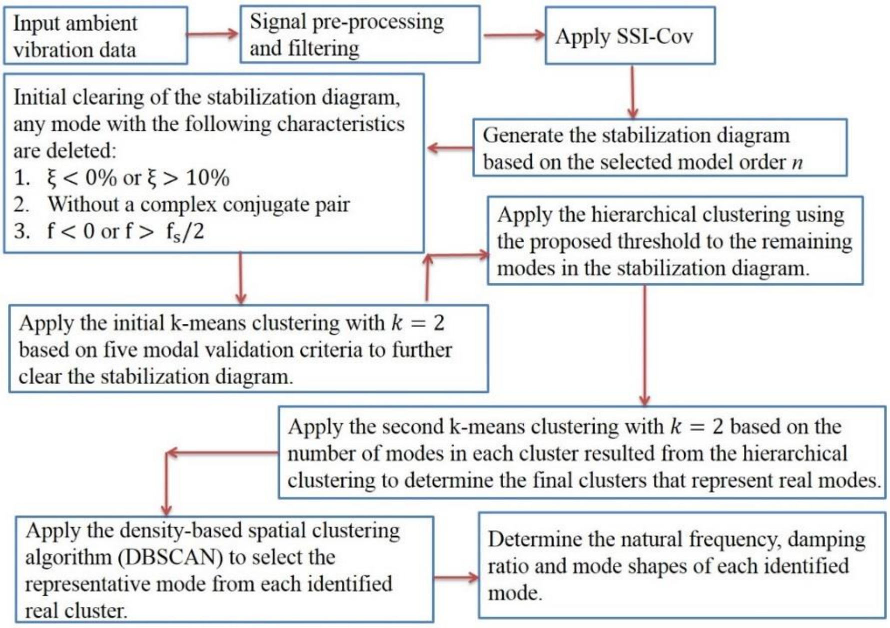

Figure 14. Illustration of SSI-Cov algorithm flowchart adopted in this work.

3.4 Reviewer 3 - Comment 4

"Please, explain why an unnecessarily high sampling frequency (600 Hz) has been adopted. Based on Figure 5 and Figure 6, I assume that data have been significantly decimated. If so, please add details about filtering and discuss the reliability of the last identified mode."

Please kindly look at the response provided to Reviewer 2 - Comment 5.

3.5 Reviewer 3 - Comment 5

"Even if I do not agree with the distinction between NExT-ERA and SSI-Cov, some inconsistencies can be identified by comparing Figures 5-6 and Table 2: for instance, the modes at 3.63 Hz and 3.68 Hz seem to be identifiable by manual identification (Figure 5a) while they are not identified by the automated OMA method (Figure 5b); the same happens for the modes at 5.71 Hz and 6.04 Hz. Moreover, the Authors should explain why the application

of two methods (that are actually the same) to the same dataset can provide very different results in terms of natural frequencies as well as damping ratios, in particular for the fundamental modes (see Table 2)."

Response:

The authors agree with the reviewer's comment that the modes at 3.63 Hz and 3.68 Hz and the modes at 5.71 Hz and 6.04 Hz were somehow visually identifiable from the uncleaned stabilization diagram presented in Figure 5 (a) of the original draft of the paper. It is worth mentioning that these modes were identified by the automated algorithm as well. However, because of the large scale of the horizontal axis (0 Hz to 60 Hz) in Figure 5 (b), closely-spaced modes might not be clearly visible to the reader. Please note that in the revised manuscript, we have replaced Table 2 and performed further investigations using new datasets. We kindly ask the reviewer to take a look at response to Reviewer 1- Comment 3.

In addition, based on the reviewer's suggestion, we have removed all the analyses performed by the ERA method and only have presented the results of SSI-Cov method in the revised manuscript.

3.6 Reviewer 3 - Comment 6

"MAC between the mode shapes estimated by the manual OMA and the automated OMA are missing but they are necessary to verify how modes are coupled for comparison, in particular in the presence of closely spaced modes as in the proposed application."

Response:

The mode shapes identified by the automated algorithm and the manual algorithm with the tolerance values of 0.010, 0.100, and 0.99, respectively, for t_f, t_ξ and MAC were used for calculation of MAC. The generated MAC matrix is shown in Figure 14. Since, the manual algorithm did not identify the ninth mode, the MAC was computed for the first eight modes. The horizontal axis represents the modes obtained from the automated algorithm and the vertical axis shows the modes identified by the manual algorithm. As seen, the diagonal MAC values are very high (>0.9) representing the high correlation between the modes obtained from the both methods. However, the closely-spaced modes 2 and 3 and modes 6 and 7 show some coupling through the off-diagonal MAC values. In general, this figure highlights the consistency of the identified modes between two methods.

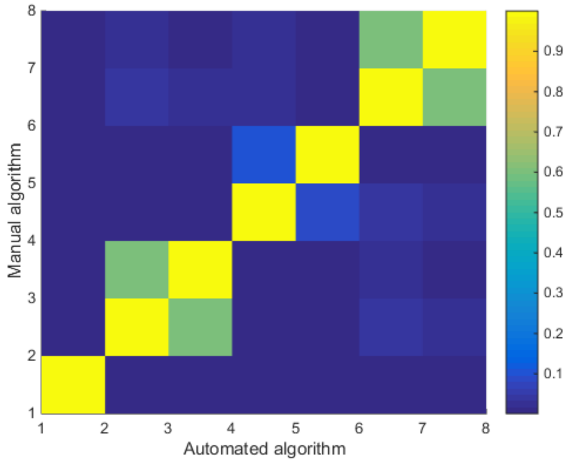

Figure 15. Orthogonality check using MAC between the identified modes from the manual and automated algorithms.

3.7 Reviewer 3 - Comment 7

“Please, explain what you mean with the sentence: "The blue curves shown in the figures are the power spectral density functions calculated using the singular values of the acceleration measurements from all 24 channels on the deck of the bridge". It is probably incorrect.”

Response:

The authors agree with the reviewer that the message has not been properly conveyed. The blue curve is indicating the first singular value of SVD (Singular Value Decomposition) of spectral density matrix at each frequency coordinate. This provides an estimate of the auto spectral density of the SDOF system in modal coordinates and the peak in the SVD curve is expected to be a structural mode.

3.8 Reviewer 3 - Comment 8

“Section 5.2 is too short and it does not add further information, while retaining the main problems reported for Section 5.1. Thus, Section 5.2 can be removed, while Section 5.1 should be extended to better demonstrate the validity of the method.”

Response:

Section 5.2 in the first draft has been eliminated. Please kindly look at the response provided to Reviewer 1 - Comment 1 and Reviewer 1 - Comment 4. Also, look at Sections 4 and 5 in the revised paper.

Reviewer 3 - Comment 9

“Additional comments: the expression "dominant modal feature" to indicate modal properties is inappropriate (line 5, pag. 2). Hermitian already include transpose, so please replace "Hermitian transpose" with "Hermitian" on pag. 6 line 10. Replace "donates" with "denotes" on line 5 pag. 8.”

Response:

These mistakes and typos were modified in the revised paper.

References

[1] Abdel-Ghaffar, A.M. and Khalifa, M.A., 1991. Importance of cable vibration in dynamics of cable-stayed bridges. Journal of Engineering Mechanics, 117(11), pp.2571-2589.

[2] Brownjohn, J., & Carden, P. (2007). Reliability of frequency and damping estimates from free vibration response. In Proceedings of the 2nd International Operational Modal Analysis Conference, (pp. 23-30).

[3] Brownjohn, J., Magalhaes, F., Caetano, E., & Cunha, A. (2010). Ambient vibration re-testing and operational modal analysis of the Humber Bridge. Engineering Structures, 2003-2018.

[4] Cantieni R. Experimental methods used in system identification of civil engineering structures. In: Proc. 1st int operational modal analysis conf (IOMAC’05); 2005.

[5] Caetano, E., Cunha, A., Gattulli, V. and Lepidi, M., 2008. Cable–deck dynamic interactions at the International Guadiana Bridge: On-site measurements and finite element modelling. Structural Control and Health Monitoring, 15(3), pp.237-264.

[6] Caetano, E., Cunha, Á. and Taylor, C.A., 2000. Investigation of dynamic cable-deck interaction in a physical model of a cable-stayed bridge. Part I: modal analysis.

[7] E. Reynders, R. Pintelon, and G. De Roeck. Uncertainty bounds on modal parameters obtained from Stochastic Subspace Identification. Mechanical Systems and Signal Processing, 22(4):948–969, 2008.

[8] Galvín, P. and Domínguez, J., 2007. Dynamic analysis of a cable-stayed deck steel arch bridge. Journal of Constructional Steel Research, 63(8), pp.1024-1035.

[9] He, X., Moaveni, B., Conte, J.P., Elgamal, A. and Masri, S.F., 2008. Modal Identification Study of Vincent Thomas Bridge Using Simulated Wind-Induced Ambient Vibration Data. Computer-Aided Civil and Infrastructure Engineering, 23(5), pp.373-388.

[10] Hermans, L. and Van der Auweraer, H., 1999. Modal testing and analysis of structures under operational conditions: industrial applications. Mechanical systems and signal processing, 13(2), pp.193-216.

[11] Kalhori, H., Alamdari M.M., Zhu, X., Samali, B., Mustapha, S., Non-intrusive schemes for speed and axle identification in bridge-weigh-in-motion systems. Measurement Science and Technology. 2017; 28 (2), 025102.

[12] Karbhari, V., & Ansari, F. (2009). Structural health monitoring of civil infrastructure systems. Elsevier.

[13] Larose, G.L., Larsen, S.V., Larsen, A., Hui, M. and Jensen, A.G., 2003, June. Sectional model experiments at high Reynolds number for the deck of a 1018 m span cable-stayed bridge. In Proceedings of the 11th International Conference on Wind Engineering (pp. 373-380).

[14] Peeters, B. and De Roeck, G., 1999. Reference-based stochastic subspace identification for output-only modal analysis. Mechanical systems and signal processing, 13(6), pp.855-878.

[15] Rainieri, C., Fabbrocino, G., Cosenza, E. and Manfredi, G., 2007, April. Implementation of OMA procedures using labview: theory and application. In 2nd international operational modal analysis conference (Vol. 30, pp. 1-13). Copenhagen: Denmark.

[16] Rainieri C, Fabbrocino G. Operational Modal Analysis of Civil Engineering Structures. New York: Springer; 2014a.

[17] Siringoringo, D.M. and Fujino, Y., 2008. System identification of suspension bridge from ambient vibration response. Engineering Structures, 30(2), pp.462-477.

[18] Turner, J.D. and Pretlove, A.J., 1988. A study of the spectrum of traffic-induced bridge vibration. Journal of Sound and Vibration, 122(1), pp.31-42.

[19] Whelan, M.J., Gangone, M.V., Janoyan, K.D. and Jha, R., 2009. Real-time wireless vibration monitoring for operational modal analysis of an integral abutment highway bridge. Engineering Structures, 31(10), pp.2224-2235.